THE JOURNAL OF BIOLOGICAL CHEMISTRY VOL. 287, NO. 41, pp. 34660–34682, October 5, 2012

Evidence for Bidirectional Endocannabinoid Transport across Cell Membranes*[S]

Received for publication, April 17, 2012, and in revised form, July 31, 2012 Published, JBC Papers in Press, August 9, 2012, DOI 10.1074/jbc.M112.373241

Andrea Chicca, Janine Marazzi, Simon Nicolussi, and Jürg Gertsch[1]

From the Institute of Biochemistry and Molecular Medicine, National Center of Competence in Research TransCure, University of Bern, CH-3012 Bern, Switzerland

Background: The transport of endocannabinoids across cell membranes is poorly understood.
Results: Using a new methodology, we provide experimental evidence for the bidirectional cell membrane transport of endocannabinoids containing an arachidonoyl chain.
Conclusion: Endocannabinoid release and uptake are regulated by a membrane-based target independent of intracellular proteins.
Significance: A specific bidirectional membrane transporter for the major endocannabinoids is postulated.

Despite extensive research on the trafficking of anandamide (AEA) across cell membranes, little is known about the membrane transport of other endocannabinoids, such as 2-arachidonoylglycerol (2-AG). Previous studies have provided data both in favor and against a cell membrane carrier-mediated transport of endocannabinoids, using different methodological approaches. Because AEA and 2-AG undergo rapid and almost complete intracellular hydrolysis, we employed a combination of radioligand assays and absolute quantification of cellular and extracellular endocannabinoid levels. In human U937 leukemia cells, 100 nM AEA and 1 μM 2-AG were taken up through a fast and saturable process, reaching a plateau after 5 min. Employing differential pharmacological blockage of endocannabinoid uptake, breakdown, and interaction with intracellular binding proteins, we show that eicosanoid endocannabinoids harboring an arachidonoyl chain compete for a common membrane target that regulates their transport, whereas other *N*-acylethanolamines did not interfere with AEA and 2-AG uptake. By combining fatty acid amide hydrolase or monoacyl glycerol lipase inhibitors with hydrolase-inactive concentrations of the AEA transport inhibitors UCM707 (1 μM) and OMDM-2 (5 μM), a functional synergism on cellular AEA and 2-AG uptake was observed. Intriguingly, structurally unrelated AEA uptake inhibitors also blocked the cellular release of AEA and 2-AG. We show, for the first time, that UCM707 and OMDM-2 inhibit the bidirectional movement of AEA and 2-AG across cell membranes. Our findings suggest that a putative endocannabinoid cell membrane transporter controls the cellular AEA and 2-AG trafficking and metabolism.

The endocannabinoid system is a lipid signaling system comprising arachidonic acid-derived ligands, such as arachidonoylethanolamide (AEA)[2] and 2-arachidonoylglycerol (2-AG), which interact with the G protein-coupled cannabinoid receptors CB_1 and CB_2 in different cell types (1, 2). The diverse roles of the endocannabinoid system (ECS) in physiological and pathological processes have been elucidated both in the central nervous system and in the periphery. In the last decade, extensive biomedical research has provided insights into how the ECS works at a mechanistic level and thus revealed new perspectives for drug discovery (1). Besides the cannabinoid receptors, the major endocannabinoid catabolic enzymes fatty acid amide hydrolase (FAAH) (3) and monoacyl glycerol lipase (MAGL) (4), several new proteins have been identified as new members of the ECS. These include the hydrolyzing enzymes *N*-acylethanolamine-hydrolyzing acid amidase (5, 6), FAAH-2 (7), α,β-hydrolase-6 and -12 (ABHD-6 and -12) (8), AEA-binding fatty acid-binding proteins (FABPs) (9), and other potential intracellular AEA carrier proteins like Hsp70 and albumin (10) and more recently the FAAH-like cytoplasmic AEA transporter (FLAT) (11). Despite an increasing knowledge about the receptors and signaling pathways involved in the ECS, the movement of AEA and 2-AG across the cell membrane remains to be elucidated and is subject to ongoing controversy (12). Previous studies have addressed the issue of intracellular AEA uptake, providing strong evidence in favor of a carrier-mediated transport that is linked to but distinctly independent of the enzymatic hydrolysis of AEA by FAAH (13–18). Importantly, sev-

* This work was supported by the Swiss National Science Foundation National Centre of Competence in Research TransCure, the University of Bern Foundation, and Novartis Research Foundation Grant 10B48.
[S] This article contains supplemental Fig. 1.
[1] To whom correspondence should be addressed. Tel.: 41-31-631-41-24; E-mail: gertsch@ibmm.unibe.ch.

[2] The abbreviations and trivial names used are: AEA, anandamide; 1-AG and 2-AG, 1- and 2-arachidonoylglycerol, respectively; ECS, endocannabinoid system; FAAH, fatty acid amide hydrolase; MAGL, monoacyl glycerol lipase; CCP, *N*-cyclohexanecarbonyl-pentadecylamine; ABHD, α,β-hydrolase; FABP, fatty acid-binding protein; FLAT, FAAH-like cytoplasmic AEA transporter; EMT, endocannabinoid membrane transporter; NADA, *N*-arachidonoyl dopamine; PEA, palmitoylethanolamide; OEA, oleoylethanlonamide; SEA, stearoylethanolamide; LEA, linoleoylethanolamide; noladin ether or 2-AGE, 2-arachidonyl glyceryl ether; PMA, phorbol 12-myristate 13-acetate; PL, phospholipid; PE, phosphatidylethanolamine; ER, endoplasmic reticulum; AIBP, AEA intracellular binding protein; AQP, aquaglyceroporin; PPAR, peroxisome proliferator-activated receptor; URB597, (3′-(aminocarbonyl)[1,1′-biphenyl]-3-yl)-cyclohexylcarbamate; UCM707, *N*-(3-furanylmethyl)-(5*Z*,8*Z*,11*Z*,14*Z*)-eicosatetraenamide; OMDM-2, (*R*)-*N*-(1-(4-hydroxyphenyl)-2-hydroxyethyl)oleamide; LY2183240, 5-[(1,1′-biphenyl]-4-yl)methyl]-*N*,*N*-dimethyl-1H-tetrazole-1-carboxamide; BMS309403, ((2′-(5-ethyl-3,4-diphenyl-1H-pyrazol-1-yl)(1,1′-biphenyl)-3-yl)oxy)-acetic acid.

eral apparently selective cellular AEA uptake inhibitors have been reported, which at nanomolar or low micromolar concentrations do not inhibit FAAH but still inhibit cellular AEA uptake (19–21). In addition to the carrier-mediated mechanism, two other models have been proposed for AEA uptake: the simple cellular diffusion driven by its fast and efficient cytoplasmic breakdown mediated by FAAH (22–25) and a carrier-mediated caveolae-related endocytotic process (26, 27). Surprisingly, few studies have addressed the uptake mechanism of 2-AG, which is the major endocannabinoid in brain and peripheral tissues (12, 28, 29). Given the strong pharmacological evidence in favor of a facilitated endocannabinoid membrane transport mechanism, the prevalent hypothesis supports the model of a putative membrane transporter (29–35). However, such an endocannabinoid membrane transporter (EMT) has not yet been identified. Moreover, it remains to be elucidated whether AEA, 2-AG, and other endocannabinoids share the same membrane transport mechanism. Another poorly investigated aspect is the process of cellular release subsequent to the biosynthesis of AEA and 2-AG at the inner membrane leaflet (36). It has been proposed that endocannabinoids are released directly from the cell membrane, where they are generated, but only few studies imply that a bidirectional membrane transporter could be involved in the release of AEA into the extracellular space (16, 37–39). Here we have experimentally addressed the issue of AEA and 2-AG cellular uptake using U937 human monocytes/macrophages. Given the complexity and pitfalls involved in the handling of endocannabinoid lipids (40, 41), we employed a combination of two independent detection methods. We used the classical radioactivity-based assays as well as a direct gas chromatography (GC)/MS-based analytical quantification of endocannabinoids. Applying this integrated methodology and using diverse combinations of pharmacological tool compounds, we have obtained data that strongly support a carrier-mediated cell membrane transport of AEA and 2-AG in U937 cells. Our results clearly suggest a common putative EMT specific for the eicosanoid endocannabinoids AEA, 2-AG, *N*-arachidonoyl dopamine (NADA), 2-arachidonyl glyceryl ether (noladin ether; 2-AGE), and *O*-arachidonoyl ethanolamine (virodhamine). This study also provides evidence that the putative EMT is mechanistically independent from the newly described AEA intracellular carrier proteins and degrading enzymes. Finally, our data strongly suggest that the putative EMT works in a bidirectional manner and also mediates the release of AEA and 2-AG. Although the EMT has not yet been cloned and identified, for the sake of clarity, we use the terms "EMT" and "EMT inhibitor," implicitly referring to the putative EMT. Overall, our study provides new evidence in favor of a membrane target that regulates the extracellular and intracellular levels of endocannabinoids in an orchestrated manner together with the cytoplasmic carrier proteins and degrading enzymes.

EXPERIMENTAL PROCEDURES

Materials—Chemicals were of the purest analytical grade. AEA, *N*-(2- hydroxyethyl-1,1,2,2-d_4)-(5*Z*,8*Z*,11*Z*,14*Z*)-eicosatetraenamide, 2-AG, (5*Z*,8*Z*,11*Z*,14*Z*)-eicosatetraenoic acid, 2-glycerol-1,1,2,3,3-d_5 ester, palmitoylethanolamide (PEA), *N*-(2-hydroxyethyl)-hexadecanamide-7,7,8,8-d_4, oleoylethanlonamide (OEA), *N*-(2-hydroxyethyl)-(9*Z*)-octadecenamide-11,11-d_2, stearoylethanolamide (SEA), linoleoylethanolamide (LEA), *N*-(2-hydroxyethyl-1,1,2,2-d_4)-(9*Z*,12*Z*)-octadecadienamide, *O*-arachidonoyl ethanolamine (virodhamine), 2-arachidonyl glyceryl ether (noladin ether), NADA, phenylmethylsulfonyl fluoride (PMSF), (3′-(aminocarbonyl)[1,1′-biphenyl]-3-yl)-cyclohexylcarbamate (URB597), *N*-cyclohexanecarbonyl-pentadecylamine (CCP), *N*-(3-furanylmethyl)-(5*Z*,8*Z*,11*Z*,14*Z*)-eicosatetraenamide (UCM707), and (*R*)-*N*-(1-(4-hydroxyphenyl)-2-hydroxyethyl)oleamide (OMDM-2) were purchased from Cayman Chemicals Europe. 5-[(1,1′-biphenyl]-4-yl)methyl]-*N*,*N*-dimethyl-1H-tetrazole-1-carboxamide (LY2183240) was purchased from Tocris Bioscience. ((2′-(5-Ethyl-3,4-diphenyl-1H-pyrazol-1-yl)(1,1′-biphenyl)-3-yl)oxy)-acetic acid (BMS309403) was purchased from Merck. [*ethanolamine*-1-^{3}H]AEA (60 Ci/mmol) and [1,2,3-^{3}H]2-AG (20–40 Ci/mmol) were obtained from American Radiolabeled Chemicals, Inc.

Cell Culture—Human monocytic leukemia U937 cells were purchased from American Type Culture Collection (Manassas, VA) and were grown in RPMI 1640 medium supplemented with 10% fetal bovine serum, 1 g/ml fungizone (amphotericin B), 100 units/ml penicillin, 100 g/ml streptomycin, and 2 mM L-glutamine (all from Invitrogen). The U937 monocytic cells were differentiated into macrophages using 2 ng/ml phorbol 12-myristate 13-acetate (PMA; Sigma) for 48 h, according to standard procedures (42–44). Cells were grown in a humidified incubator at 37 °C and 5% CO_2 at 37 °C in humidified 5% CO_2 atmosphere.

Radioactivity-based Determination of Endocannabinoid Uptake—The uptake of [*ethanolamine*-1-^{3}H]AEA (60 Ci/mmol) and [1,2,3-^{3}H]2-AG, (20–40 Ci/mmol) in intact cells was performed by using U937 and PMA-differentiated U937 (macrophage) cells. Briefly, 10^6 cells were suspended in 500 μl of serum-free medium in silanized plastic tubes and preincubated with different concentrations of inhibitors for 10–30 min at 37 °C, depending on the experiment. Plastic or glass tubes were filled with AquaSil™ siliconizing fluid (ThermoScientific), and after 1 min, the silanizing agent was removed and discarded. The tubes were rinsed with pure methanol and then allowed to dry overnight at room temperature. Combination experiments were performed by co-preincubating the cells with both FAAH and EMT inhibitors. Successively, cells were added with a mixture of either AEA/[^{3}H]AEA to a final concentration of 100 nM or 2-AG/[^{3}H]2-AG to a final concentration of 1 μM and then incubated for 5 min at 37 °C. Time course experiments were performed by incubation of the cells from 30 s to 60 min. In AEA plus 2-AG and AEA and/or 2-AG plus other lipids (endocannabinoids or *N*-acylethanolamines) combination experiments, the endocannabinoids were co-incubated for 5 min with the cells without preincubation. The uptake process was stopped by transferring the tubes on ice and rapidly centrifuging them at 800 × *g* for 5 min at 4 °C. The supernatant was collected (500 μl) and transferred into 1 ml of a methanol/chloroform mixture (1:1, v/v), whereas the pellet was resuspended in ice-cold PBS plus 1% fatty acid-free BSA and centrifuged at 800 × *g* for 5 min at 4 °C (washing step). The washing solution was collected and the radioactivity measured together

with the extracellular organic phase. The cell pellet was resuspended in 250 μl of ice-cold PBS and transferred into 500 μl of a methanol/chloroform mixture (1:1, v/v), vortexed vigorously, sonicated in an ice-cold water bath for 5 min, and finally centrifuged at 10,000 rpm for 10 min at 4 °C. The aqueous phase was pooled with the aqueous phase extracted from the supernatant and transferred in a scintillation tube, whereas the lipophilic phase was transferred in a different tube. The radioactivity measured in the pooled aqueous phases represented the amount of [^{3}H]ethanolamine or [^{3}H]glycerol generated by [^{3}H]AEA or [^{3}H]2-AG hydrolysis, respectively. The intracellular and extracellular amount of [^{3}H]AEA and [^{3}H]2-AG as well as the [^{3}H]glycerol and [^{3}H]ethanolamine formation were measured by adding 3 ml of Ultima Gold scintillation liquid (PerkinElmer Life Sciences) using a Packard Tri-Carb 2100 TR scintillation counter (PerkinElmer Life Sciences). Data were collected from at least three independent experiments performed in triplicate, and results were expressed as [^{3}H]ethanolamine (or [^{3}H]glycerol) formation and intracellular or extracellular [^{3}H]AEA (or [^{3}H]2-AG) reduction or accumulation in percentage of the vehicle-treated samples.

Construction of Theoretical Curves for Additivity and Independent Interaction—In order to investigate the type of interaction between EMT and FAAH inhibitors, when applied in combination to the cells, we made use of an empirical method previously described by Pöch *et al.* (45–48). This method allows analysis of the combination of increasing concentrations of a compound A (the FAAH inhibitors URB597 and PMSF) in the presence of a fixed concentration of the compound B (the EMT inhibitor UCM707 at 1 μM or OMDM-2 at 5 μM). The construction of the theoretical curves is based upon the assumption that A and B contribute to the overall effect, either interacting on the same target or on two different targets. In the first case, it is assumed that B behaves like A, thus interacting at the same target. This leads to the construction of the theoretical curve for additivity. In this case, B can be seen as a dilution of A, which is equieffective with a certain concentration of A, termed *x*. Based on this assumption, the expected effects of the combination A + B represent the effects of A + *x* (where *x* is the concentration of A that is equieffective to B). As a consequence, the theoretical curve for additivity is constructed by replotting the concentration curve of A to the left of the original curve by a distance *x*. In line with the definition of the additivity given above, at the highest concentration of A, the E_{max} reached by the combination A + B does not differ from the one obtained by applying only A. The construction of the theoretical curve for "independent interaction" is based on the assumption that A and B act independently on two distinct targets. This curve is constructed by using Equation 1,

$$E_{A+B} = E_A + E_B - (E_A \times E_B) \quad \text{(Eq. 1)}$$

where the E_{max} is 1. Thus, the response to A + B is expressed as a fraction of the maximum frequency. If the interaction between A and B is independent, the theoretical curve will appear upward shifted compared with the concentration-effect curve of A. The magnitude of such a shift is determined by the response to B. The independent interaction is also called "functional synergy" (48).

Radioactivity-based Determination of Endocannabinoid Release—The release of [*ethanolamine*-1-^{3}H]AEA (60 Ci/mmol) and [1,2,3-^{3}H]2-AG (20–40 Ci/mmol) was carried out in U937 cells. Briefly, 10^6 cells were suspended in 500 μl of serum-free medium in silanized plastic tubes and preincubated for 30 min at 37 °C with a degrading enzyme inhibitor mixture in order to block AEA and 2-AG hydrolysis. 100 nM URB597 plus 1 μM PMSF was used to fully avoid AEA cleavage, whereas a mix of 1 μM JZL184, 10 μM WWL70, and 20 μM tetrahydrolipstatin was used to block 2-AG breakdown. Afterward, cells were loaded with a mix of "cold/hot" endocannabinoid through a 5-min incubation at 37 °C to allow the cells to intracellularly accumulate the molecules. Next, the cells were centrifuged for 5 min at 800 × *g*, the supernatant was discarded, and a washing step with PBS plus 1% BSA was performed in order to eliminate the residual endocannabinoid molecules stuck on the external plasma membrane leaflet. After a subsequent centrifugation step, cells were resuspended in endocannabinoid-free PBS containing 1% fatty acid free BSA as AEA and 2-AG extracellular acceptor and incubated for 25 min at 37 °C. Finally cells were centrifuged at 800 × *g* for 5 min at 4 °C, and the pellet and the supernatant underwent an aqueous/organic separation phase as described above. The radioactivity associated with the intracellular and extracellular [^{3}H]AEA and [^{3}H]2-AG was measured by adding 3 ml of Ultima Gold scintillation liquid (PerkinElmer Life Sciences) using a Packard Tri-Carb 2100 TR scintillation counter (PerkinElmer Life Sciences). The radioactivity of the aqueous phase was measured to confirm the absence of endocannabinoid hydrolysis. Data were collected from at least three independent experiments performed in triplicate, and results were expressed as [^{3}H]AEA (or [^{3}H]2-AG) intracellular and extracellular levels as a percentage of the vehicle-treated samples.

FAAH Activity—FAAH activity was assessed by using either pig brain or U937 cell homogenates, as described previously (49). Briefly, 10 μl of the inhibitor at the adequate concentration or vehicle control was preincubated for 15 min at 37 °C with 490 μl of diluted pig brain (200 μg/sample) or U937 cell homogenates (corresponding to 10^6 cells = 0.63 mg of total protein) in 10 mM Tris-HCl, 1 mM EDTA, pH 8.0, plus 0.1% fatty acid-free BSA. A mixture of 100 nM AEA plus [^{3}H]AEA was added to the samples and incubated for 15 min at 37 °C. Successively, 1 ml of methanol/chloroform mixture (1:1, v/v) was added, and after vigorous vortexing, the aqueous and organic phases were separated by centrifugation at 10,000 rpm for 10 min at 4 °C. The radioactivity associated with the [^{3}H]ethanolamine was measured upon the addition of 3 ml of Ultima Gold scintillation liquid (PerkinElmer Life Sciences) to the aqueous phase, using a Packard Tri-Carb 2100 TR liquid scintillation analyzer. Results were expressed as percentage of FAAH activity *versus* vehicle-treated homogenate.

Quantification of AEA and 2-AG Levels by GC/MS—After incubation with the compounds, cells were pelleted by centrifugation at 800 × *g*, and supernatant was removed. Cell pellets were subsequently washed with 1% fatty acid-free BSA and again centrifuged at 800 × *g* at 4 °C. Both supernatants were combined for extraction, and for quantification; the cells were

analyzed separately. The quantification of the AEA and 2-AG levels was performed according to our recently published method (50).

Lipid Extraction—Cell pellets were resuspended into 250 μl of PBS and transferred to 1.5 ml of ice-cold chloroform/methanol mixture (2:1, v/v) containing internal standards yielding a 4:2:1 ratio ($CHCl_3/CH_3OH/H_2O$, v/v/v) (51). The suspension was vortexed vigorously, sonicated for 5 min in an ice-cold water bath and then centrifuged for 10 min at 500 $\times$ *g* at 4 °C. The organic phase was recovered into a glass vial, dried under N_2 reconstituted in 1 ml of ethanol, diluted with 9 ml of water, and finally extracted by solid-phase extraction (C-18 Sep-Pak cartridge (Waters AG, Baden-Dättwil, Switzerland)). Supernatants were diluted in 1 ml of ethanol (containing internal standards), and water was added to reach the final volume of 10 ml. The lipids were extracted by solid-phase extraction (C-18 Sep-Pak cartridge (Waters AG)). The internal standards used for the quantification were as follows: *N*-arachidonoylethanolamine-d_4 (1 ng/μl) (25 ng/sample) and 2-arachidonoylglycerol-d_5 (8 ng/μl) (200 ng/sample).

Derivatization and GC/MS Conditions—Derivatization of the hydroxyl groups was performed with the silylating agent dimethylisopropylsilyl imidazole at room temperature for 1 h as reported previously (52). Samples were subjected to a Sephadex LH-20 column and eluted with hexane/chloroform/methanol (10:10:1). After evaporation to dryness, samples were resuspended in 25 μl of hexane and subsequently analyzed by GC/electron ionization mass spectrometry using an Agilent 6890 N gas chromatograph equipped with a 30-meter HP-5MS column and a 5975 C electron ionization mass spectrometer with a triple-axis detector. Helium was used as the carrier gas at a constant flow rate of 1.5 ml/min with splitless injection at an inlet temperature of 250 °C. Optimal separation of the analytes was achieved with the following oven program: initial temperature 150 °C for 1 min followed by an increase to 280 °C at 8 °C/min with a final time of 20 min. Due to acyl group migration of 2-AG during lipid extraction and purification, a significant amount of 1-AG was formed. Therefore, the peak areas of 1-AG and 2-AG were combined for all quantifications as already described (53).

Thin Layer Chromatography (TLC) Analysis—U937 cells or U937 macrophages (10^6) were suspended in 500 μl of serum-free medium in silanized plastic tubes and incubated with different concentrations of [^{3}H]AEA or [^{3}H]2-AG for 5 min at 37 °C, depending on the experiment. Afterward, the cells were centrifuged for 5 min at 800 $\times$ *g* at 4 °C. Supernatants were collected, and cell pellets were resuspended in 250 μl of PBS and transferred to 1.5 ml of ice-cold chloroform/methanol mixture (2:1, v/v). The suspension was vortexed vigorously, sonicated for 5 min in an ice-cold water bath, and centrifuged for 10 min at 500 $\times$ *g*. Organic and aqueous phases were separated and dried under N_2. The organic phase was reconstituted in 10 μl of chloroform, and the aqueous phase was reconstituted in 5 μl of water and applied to the TLC plate. The same procedure was carried out for the supernatant.

Lipids were separated by one-dimensional TLC on Silica Gel 60 plates (Merck) in a solvent system composed of chloroform/methanol/acetic acid/water (25:15:4:2, v/v/v/v) and visualized by exposure to iodine vapor. The radioactive lipids were detected on dried TLC plates using a radioisotope detector (Berthold Technologies) and quantified by using the Rita Control software provided by the manufacturer.

RT-PCR Analyses of ABHDs—Total RNA was extracted from U937 cells and U937 macrophages, and mRNA was reverse-transcribed as described previously (54). cDNA samples were amplified for 35 cycles: 1 min at 95 °C; 1 min at 64.1 °C (ABHD-6), 70 °C (ABHD-12), or 55 °C (GAPDH); 1 min at 72 °C plus an elongation step at 72 °C for 10 min. Primers used were 5′-GCTCAGTGTGGTCAAGTTCCTTCCA-3′ (forward) and 5′-TTCCATCACTACTGAGTGCCCACAG-3′ (reverse) for ABHD-6; 5′-GGGTGACTCAGTGGGAACGCC-3′ (forward) and 5′-GCTGCTGACTGGAGGAAAACGGG-3′ (reverse) for ABHD-12; 5′-GTGAAGGTCGGTGTCAACG-3′ (forward) and 5′-GGTGAAGACGCCAGTAGACTC-3′ (reverse) for GAPDH. The expected amplification products were 673-, 638-, and 300-bp-long, respectively. ABHD-6 and -12 primers were designed by Oligo-Primer Analysis Software version 4.0, whereas GAPDH primer sequences were as published previously (54).

Statistical Analysis—Results are expressed as mean values ± S.E. of at least three independent experiments performed in triplicate. Statistical significance of differences between groups was determined by Student's *t* test (unpaired *t* test) with GraphPad Prism version 5 software. Statistical significance was evaluated using two-tailed unpaired *t* tests against controls. Differences between the analyzed samples were considered as significant if p was ≤ 0.05.

RESULTS

AEA and 2-AG Uptake Kinetics and Reincorporation into Phospholipids—First, the kinetics of [^{3}H]AEA and [^{3}H]2-AG uptake into human monocyte-like U937 cells was evaluated in the time range from 30 s to 60 min. U937 cells have previously been reported to exhibit good AEA uptake (K_m value ~0.2 μM) (55). The data shown in Fig. 1 clearly indicate that both molecules are taken up through a fast and saturable process and undergo a rapid and almost complete intracellular hydrolysis. The intracellular [^{3}H]AEA and [^{3}H]2-AG levels, as well as their hydrolytic products formed, showed a hyperbolic increase over time, reaching a plateau after ~5 min of incubation. Accordingly, the extracellular clearance of [^{3}H]AEA and [^{3}H]2-AG followed the mirrored hyperbolic trend (Fig. 1, *A* and *B*). In both endocannabinoids the ^{3}H labels were in the headgroup of the lipid, which is ethanolamine for AEA and glycerol for 2-AG. Interestingly, upon methanol/chloroform phase separation, the level of glycerol was more than double the ethanolamine level at each time point, whereas the intracellular amount of the relative endocannabinoid precursor showed an opposite trend, with AEA being more than double the 2-AG level. In order to investigate this unexpected difference, we performed TLC analyses of the intra- and extracellular sources of the radioactive signal. Although it has previously been reported that ethanolamine generated upon [^{14}C]AEA hydrolysis in RBL-2H3 rat basophilic leukemia cells is not incorporated into membrane phospholipids (PLs) (25), our results clearly show a significant incorporation of [^{3}H]ethanolamine into U937 membrane phos-

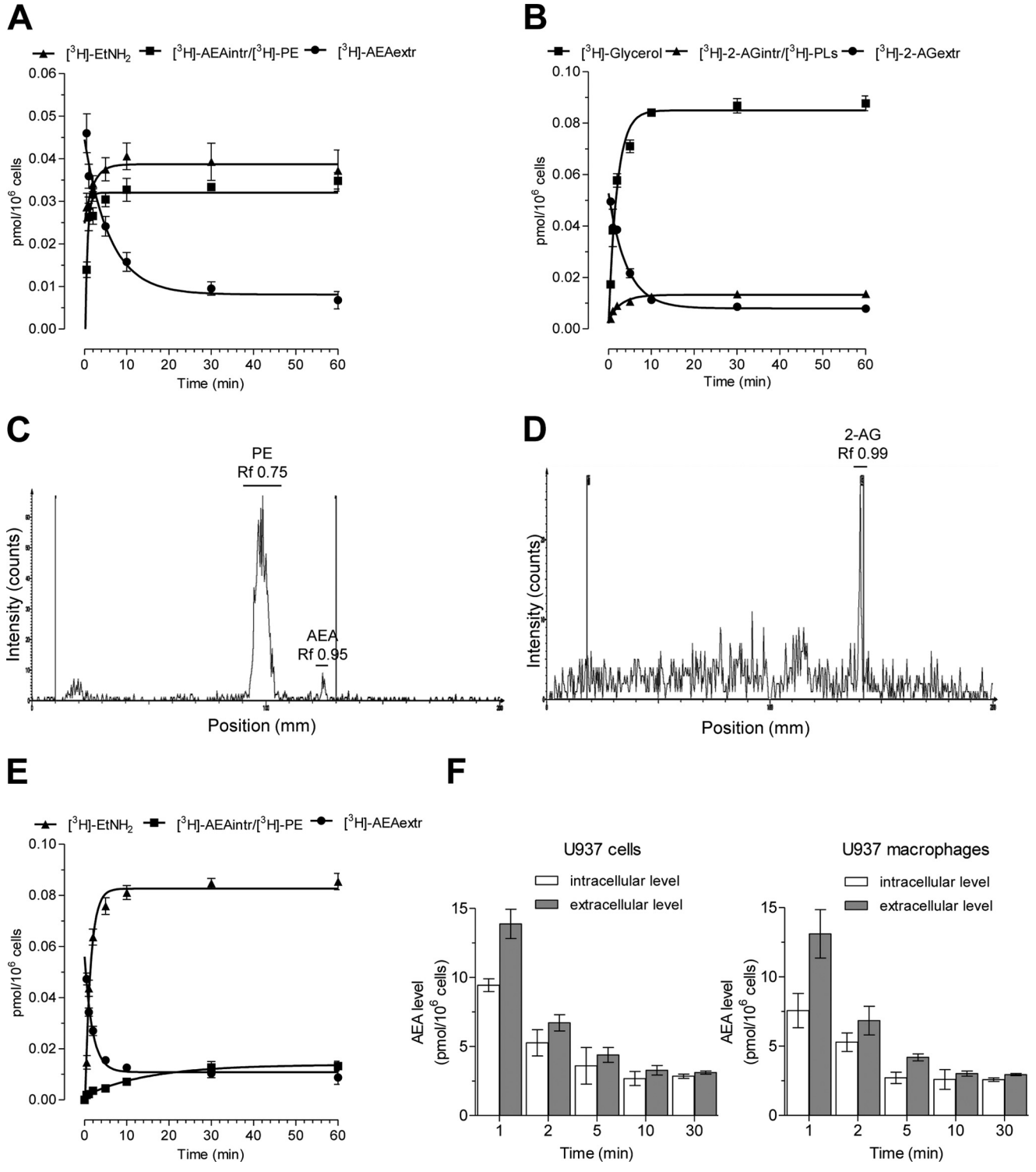

FIGURE 1. **Kinetic measurements (30 s to 60 min) of the intracellular and extracellular AEA and 2-AG levels.** *A*, time-dependent increase of intracellular [^{3}H]AEA (*AEAintr*), decrease of extracellular [^{3}H]AEA (*AEAextr*) and [^{3}H]ethanolamine (*EtNH$_2$*) formation after incubation of 100 nM [^{3}H]AEA plus AEA in U937 cells (10^6 cells). *B*, time-dependent increase of intracellular [^{3}H]2-AG (*2-AGintr*), decrease of extracellular [^{3}H]2-AG (*2-AGextr*), and [^{3}H]glycerol formation after the incubation of 1 μM [^{3}H]2-AG plus 2-AG with U937 cells (10^6 cells). *C*, TLC analysis of the cellular radioactivity originating from the addition of [^{3}H]AEA in U937 cells. Most of the radioactivity was found in PE-incorporated [^{3}H]ethanolamine and only little as intact [^{3}H]AEA. *D*, TLC analysis of the cellular radioactivity originating from the addition of [^{3}H]2-AG in U937 cells. Almost all of the radioactivity was found as intact [^{3}H]2-AG. *E*, time-dependent increase of intracellular [^{3}H]AEA, decrease of extracellular [^{3}H]AEA, and [^{3}H]ethanolamine formation after the incubation of 100 nM of [^{3}H]AEA plus AEA in U937 cells. *F*, kinetic measurement (1–30 min) of the absolute intracellular and extracellular AEA levels after the incubation of 100 nM AEA in U937 cells and U937 macrophages (10^6 cells). The values are expressed as pmol of AEA, 2-AG, EtNH$_2$, or glycerol per 10^6 cells. The radioactive signal for [^{3}H]ethanolamine and [^{3}H]glycerol represents the sum of the radioactivity recovered in the aqueous phases coming from cells and supernatant. Data show mean values ± S.E. (*error bars*) of three independent experiments, each one carried out at least in triplicates.

TABLE 1

Intra- and extracellular sources of ^{3}H signal measured after 5 min of incubation with either 100 nM [^{3}H]AEA plus AEA or 1 μM [^{3}H]2-AG plus 2-AG with U937 cells and U937 macrophages

The values are expressed as a percentage of the total ^{3}H signal. Values are expressed as means of three independent experiments, each one carried out at least in triplicate. S.E. was always less than 5% of the mean.

Cell type	[^{3}H]AEA$_{intr}$	[^{3}H]PE	[^{3}H]AEA$_{extr}$	[^{3}H]Ethanolamine
	%	%	%	%
U937 cells	2.5	74.9	18.1	4.5
U937 macrophages	0.5	4.8	10.8	83.9
	[^{3}H]2-AG$_{intr}$	[^{3}H]PLs	[^{3}H]2-AG$_{extr}$	[^{3}H]Glycerol
	%	%	%	%
U937 cells	4.1	0.2	0.8	94.9
U937 macrophages	3.8	0.4	1.3	94.5

pholipids. As shown in Fig. 1*C*, the bulk of the intracellular radioactive signal after 5 min of incubation did not originate from intact [^{3}H]AEA but from [^{3}H]ethanolamine incorporated into phosphatidylethanolamine (PE). The retardation factors of the different PLs and endocannabinoids and degrading products were determined on TLC (data not shown). On the other hand, TLC analyses of U937 cells incubated with [^{3}H]2-AG did not reveal any significant incorporation of [^{3}H]glycerol into PLs (Fig. 1*D*). In Table 1, the relative contributions (expressed as a percentage of the total radioactive signal) of the radioactive sources show that 74.9 and 0.2% of intracellular radioactivity come from PL-incorporated [^{3}H]ethanolamine and [^{3}H]glycerol, respectively. Therefore, free [^{3}H]glycerol accounts for almost 95% of the total radioactive signal, whereas free ethanolamine has only a minor contribution (less than 5%). The [^{3}H]ethanolamine was detected both intracellularly and extracellularly, whereas [^{3}H]glycerol was recovered almost only extracellularly (data not shown). We performed the same kinetic experiments in differentiated non-proliferating U937 macrophages (obtained by treating U937 cells with 2 ng/ml PMA for 48 h). U937 macrophages showed the same hyperbolic time-dependent increase of the intracellular radioactive signal. However, the intracellular radioactivity was 4 times lower in macrophages than in U937 cells at each time point, whereas the [^{3}H]ethanolamine level was more than double (Fig. 1*E*). The time-dependent extracellular AEA clearance showed the same qualitative and quantitative trend in both cell types (Fig. 1, *A* and *E*). In agreement with this, TLC analyses revealed a remarkable difference in the [^{3}H]ethanolamine incorporation into PLs because non-proliferating U937 macrophages showed low [^{3}H]PE levels (5% of total radioactivity signal) in comparison with U937 cells (Table 1). No difference was observed in the 2-AG levels and glycerol formation over time between the two cells types (Table 1).

Based on the above observations, we concluded that the intracellular fate of endocannabinoids and their hydrolytic products has to be taken into consideration when approaching the trafficking and degradation issues. Because experiments using radiolabeled endocannabinoids may be ambiguous due to differential phospholipid incorporation, we assessed the uptake kinetics of AEA and 2-AG by quantifying their absolute levels by GC/MS. The intracellular AEA level was very high already after 1 min of incubation and then dramatically decreased over time, reaching the plateau after 5 min (Fig. 1*F*). The absolute quantification of AEA therefore confirmed the rapid uptake and subsequent intracellular degradation and ethanolamine incorporation into PE. The absolute AEA quantification was performed also in U937 macrophages showing exactly the same kinetics for intra- and extracellular AEA levels (Fig. 1*F*). Thus, depending on the cell type, the incorporation of [^{3}H]ethanolamine into PE can significantly alter the readout. The same GC/MS experiments were performed using 2-AG, but it was not possible to measure any intra- or extracellular levels because 2-AG was below the limit of detection at every time point (data not shown), possibly reflecting its very rapid enzymatic breakdown at the U937 cell membrane.

Independent Interaction between EMT and FAAH Inhibitors upon Cellular Uptake of AEA—To explore the membrane-specific endocannabinoid transport mechanisms, the effects of the commercially available EMT inhibitors UCM707 (20) and OMDM-2 (19) as well as the FAAH inhibitors URB597 (56) and PMSF (57) on AEA uptake were tested alone or in combination in U937 cells. First, the IC_{50} values of UCM707 and OMDM-2 were calculated. In agreement with the literature (19, 20), the IC_{50} values were 1.8 and 5.2 μM, respectively (Fig. 2, *A* and *B*). Similarly, we measured the effects of URB597 and PMSF on AEA uptake and degradation in U937 cells (Fig. 2, *C* and *D*). Because the enzyme *N*-acylethanolamine-hydrolyzing acid amidase can be involved in AEA breakdown (5, 6), we also tested the *N*-acylethanolamine-hydrolyzing acid amidase-selective inhibitor CCP in U937 cell homogenate. CCP did not show any effect on AEA degradation up to 30 μM. Accordingly, CCP did not affect AEA uptake in U937 cells up to 30 μM (data not shown). On the other hand, URB597 and PMSF led to an extracellular accumulation of [^{3}H]AEA and a reduction of the intracellular [^{3}H]AEA/[^{3}H]PE levels and the [^{3}H]ethanolamine formation (Fig. 2, *C* and *D*). We then chose an EMT inhibitor concentration that produced a 30–40% reduction of AEA uptake (1 μM for UCM707 and 5 μM for OMDM-2) to combine with different concentrations of FAAH inhibitors. Both UCM707 and OMDM-2 have been shown to specifically inhibit the cellular uptake of AEA up to concentrations of 10 and 30 μM, respectively, whereas at higher concentrations, they also inhibited FAAH activity (19, 20). Our data confirmed that UCM707 and OMDM-2 at 1 and 5 μM, respectively, did not inhibit FAAH activity in pig brain homogenate and U937 cells homogenate (Table 2). In addition, we monitored the kinetics of the AEA uptake inhibition mediated by the two EMT inhibitors. The data showed identical inhibitory potencies from 30 s to 10 min of incubation (Fig. 2*E*), suggesting that these molecules bind to a plasma membrane target which regulates AEA entry, thus blocking endocannabinoid uptake independently from the intracellular targets involved in the later phases of AEA trafficking (see also below).

In the combination experiments, 1 μM UCM707 and 5 μM OMDM-2 were co-incubated with increasing concentrations of FAAH inhibitors, and the cells were subsequently incubated with 100 nM AEA containing 0.5% [^{3}H]AEA for 5 min. As shown in Fig. 3, *A–D*, the intracellular levels of [^{3}H]AEA/PE was significantly reduced by the combination as compared with the inhibition induced by the FAAH inhibitor alone, leading to the assumption that the two compounds may act synergistically

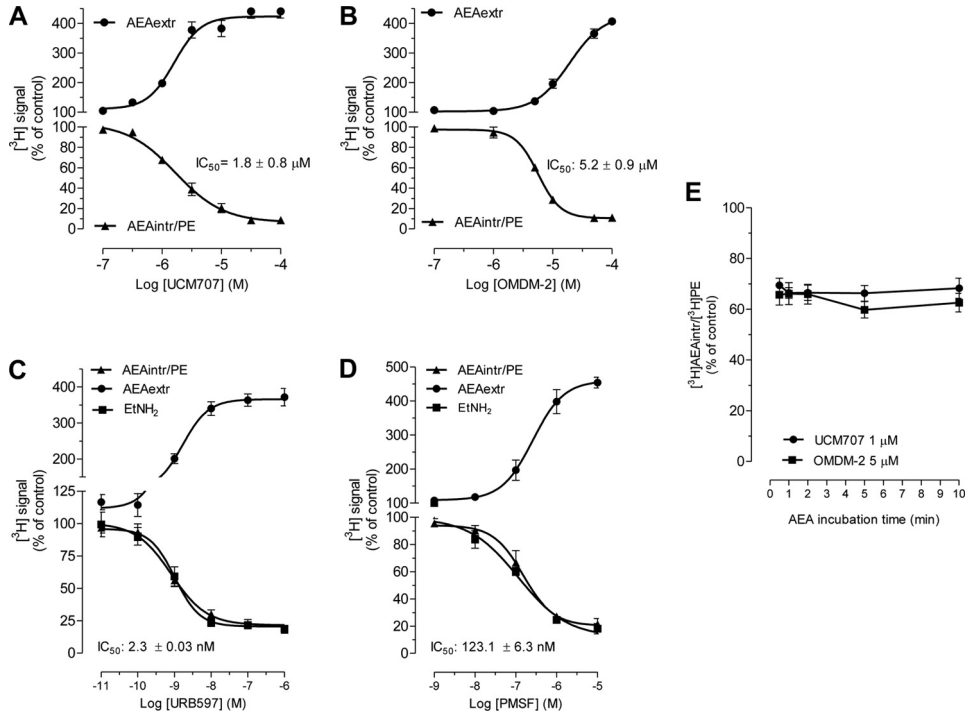

FIGURE 2. *A–D*, cellular [^{3}H]AEA uptake inhibition and extracellular [^{3}H]AEA accumulation after 5-min incubation with 100 nM [^{3}H]AEA plus AEA and 20-min pretreatment with UCM707 (*A*), OMDM-2 (*B*), URB597 (*C*), and PMSF (*D*) in U937 cells (10^6 cells). For URB597 (*C*) and PMSF (*D*), the [^{3}H]ethanolamine ($EtNH_2$) inhibition curve is also shown. The IC_{50} values were calculated from the AEA uptake inhibition curves. *E*, kinetic measurement of [^{3}H]AEA uptake inhibition calculated after different times of incubation (from 30 s to 10 min) with 100 nM [^{3}H]AEA plus AEA and 20-min pretreatment with 1 μM UCM707 or 5 μM OMDM-2 in U937 cells (10^6 cells). All values are expressed as a percentage of vehicle-treated control. The values are expressed as mean ± S.E. (*error bars*) of three independent experiments, each carried out in at least triplicates. No statistically significant difference was observed in the inhibition potency of 1 μM UCM707 (~32%) and 5 μM OMDM-2 (~40%) in the whole time range.

TABLE 2

Percentage of FAAH activity inhibition induced by 1 μM UCM707 and 5 μM OMDM-2

The values are expressed as a percentage of vehicle-treated control. The values are expressed as the mean of three independent experiments, each one carried out at least in triplicate. S.E. was always less than 5% of the mean.

Compound	U937 cell homogenate (10^6 cells)	Pig brain homogenate (200 μg of total protein)
	%	%
UCM707 (1 μM)	0	0
OMDM-2 (5 μM)	8	10

by inhibiting two distinct targets (*i.e.* FAAH and the EMT). In order to test this hypothesis, we constructed two theoretical curves (see "Experimental Procedures"), assuming either a common target for the FAAH and endocannabinoid cell membrane transport inhibitors (theoretical additive curve) or two distinct targets (theoretical curve for independent interaction). As shown in Fig. 3, *A–D*, we calculated both theoretical curves for AEA uptake inhibition (shown by *dotted lines*) by 1 μM UCM707 and 5 μM OMDM-2 with increasing concentration of FAAH inhibitor. The experimental combination of a fixed concentration of the inhibitor of AEA transport with increasing concentrations of the FAAH inhibitor is described by a sigmoidal curve that resembles the theoretical curve for independent interaction. As shown in Fig. 3, *A–D*, the inhibition curves for combinations were shifted upward compared with the FAAH inhibitor curves. Thus, the [^{3}H]AEA/PE intracellular levels measured after the treatment with the combinations are significantly lower than the levels measured after the treatment with FAAH inhibitors. In line with the independent interaction model, the E_{max} reached with the combinations is significantly higher than the E_{max} obtained with URB597 and PMSF alone, in agreement with the assumption of two different targets (see Fig. 3, *A–D*). Furthermore, at very low and almost FAAH-ineffective concentrations of URB597 (10–100 pM) and PMSF (1–10 nM), the effects of the combination on the intracellular [^{3}H]AEA/PE level were much stronger than the theoretical curves, except for the OMDM-2/URB597 combination (Fig. 3, *A–D*). The IC_{50} values calculated from the inhibition curves of URB597 and PMSF alone or in the presence of 1 μM UCM707 or 5 μM OMDM-2 is reported in Table 3.

In agreement with the uptake inhibition data, the extracellular [^{3}H]AEA accumulation measured after treating the cells with combinations of EMT and FAAH inhibitors was significantly higher than the effect obtained applying FAAH inhibitors alone. In particular, for low and FAAH-ineffective concentrations of URB597 and PMSF, the extracellular [^{3}H]AEA levels were higher than the expected levels for 1 μM UCM707 (≅280% *versus* 197% of control for combinations and UCM707, respectively) and for 5 μM OMDM-2 (≅180% *versus* 138% of control for the OMDM-2/PMSF combination and OMDM-2, respectively), again supporting an independent effect between EMT and FAAH inhibitors (Fig. 3, *E–H*).

The same set of experiments were carried out by adding only AEA without [^{3}H]AEA and quantifying the absolute intracellular and extracellular levels by GC/MS. As shown in Fig. 4, treatment with UCM707 or OMDM-2 induced a reduction of AEA uptake similar to the one observed in the radioactivity-based

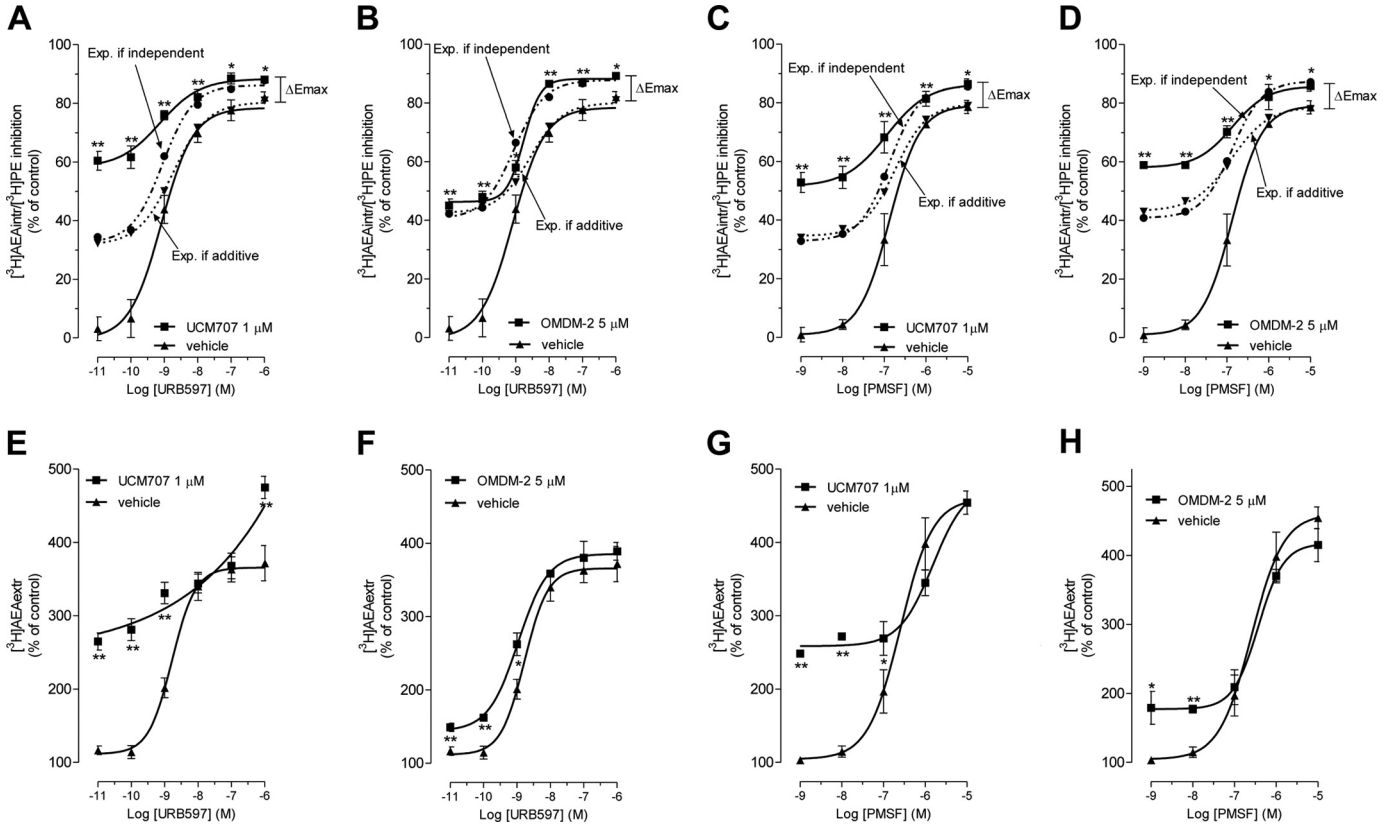

FIGURE 3. **Concentration-dependent [^{3}H]AEA uptake inhibition induced by FAAH inhibitors alone or in combination with UCM707 or OMDM-2.** Cellular [^{3}H]AEA uptake inhibition after a 5-min incubation of 100 nM [^{3}H]AEA plus AEA and 20-min pretreatment with URB597 alone and in the presence of 1 μM UCM707 (*A*) or 5 μM OMDM-2 (*B*) in U937 cells (10^6 cells). In every graph, the theoretical curves for additivity and independent interaction are shown as *dotted lines*. Curves were calculated, applying a model based on the assumption that the two compounds act either on the same target (additivity) or on different targets (independent interaction). See "Experimental Procedures" for details. The same [^{3}H]AEA uptake inhibition curve was measured after a 20-min pretreatment with PMSF alone or in the presence of 1 μM UCM707 (*C*) or 5 μM OMDM-2 (*D*). The concentration-dependent extracellular [^{3}H]AEA accumulation measured in the same experimental conditions is shown for URB597 alone and in the presence of 1 μM UCM707 (*E*) or 5 μM OMDM-2 (*F*) and for PMSF alone and in the presence of 1 μM UCM707 (*G*) or 5 μM OMDM-2 (*H*). The values are expressed as a percentage of cellular or extracellular [^{3}H]AEA levels as compared with vehicle-treated control. Data show mean values ± S.E. (*error bars*) of three independent experiments, each one carried out at least in triplicate. *, $p < 0.05$; **, $p < 0.01$, combination treatment *versus* URB597 or PMSF alone.

TABLE 3

IC_{50} values for AEA uptake inhibition calculated after a 5-min incubation with 100 nM [^{3}H]AEA plus AEA and 20-min pretreatment with URB597 and PMSF alone or in the presence of UCM707 or OMDM-2 in U937 cells

The IC_{50} values are expressed as a percentage of vehicle-treated control. The values are expressed as mean ± S.E. of three independent experiments, each one carried out at least in triplicate.

Compounds/combinations	AEA uptake inhibition (IC_{50}) ± S.E.
	nM
URB597	2.3 ± 0.03
URB597 + UCM707 (1 μM)	<0.01 ± 0.002
URB597 + OMDM-2 (5 μM)	0.01 ± 0.002
PMSF	123.1 ± 6.3
PMSF + UCM707 (1 μM)	1.0 ± 0.07
PMSF + OMDM-2 (5 μM)	<1.0 ± 0.01

assays. In contrast, however, URB597 and PMSF led to a significant increase of the intracellular AEA level because in the vehicle control, the incorporation of ethanolamine did not lead to an overestimation of the intracellular AEA level (see Fig. 1). When cells were treated with a combination of EMT and FAAH inhibitors, the increase of intracellular AEA was abolished (Fig. 4, *A* and *B*). Thus, when the AEA cellular uptake was inhibited, the FAAH inhibition effects by PMSF and URB597 were not seen. This provides very strong evidence in favor of a membrane transporter. Moreover, UCM707 and OMDM-2 showed identical inhibition of AEA uptake irrespective of the presence of PMSF and URB597 (Fig. 4, *A* and *B*). In agreement, the extracellular level of AEA was increased by all of the treatments (EMT inhibitors, FAAH inhibitors, and combinations) (Fig. 4, *C* and *D*). Overall, these data clearly indicate that a putative EMT is involved in the first step of AEA cellular uptake.

UCM707 or OMDM-2 Inhibits AEA Uptake without Interfering with FABPs—The degradation of AEA and 2-AG is mediated by several enzymes located in different cellular compartments. 2-AG hydrolysis is catalyzed mainly by MAGL, a soluble enzyme, which has been found to be associated with the inner cell membrane layer and the recently identified ABHD-6 and ABHD-12, which have been proposed to be integral cell membrane proteins with the catalytic site facing intra- and extracellularly, respectively (58, 59). Therefore, 2-AG hydrolysis seems to occur almost exclusively at the cell membrane. On the contrary, the main enzyme involved in the AEA degradation is FAAH, whose localization has been described primarily in the endoplasmic reticulum (ER) (3). Once AEA is taken up into the cell, it needs to travel across the cytosol to reach the ER, where it is finally cleaved. AEA is a lipophilic molecule that is not able to move freely across the hydrophilic cytosolic envi-

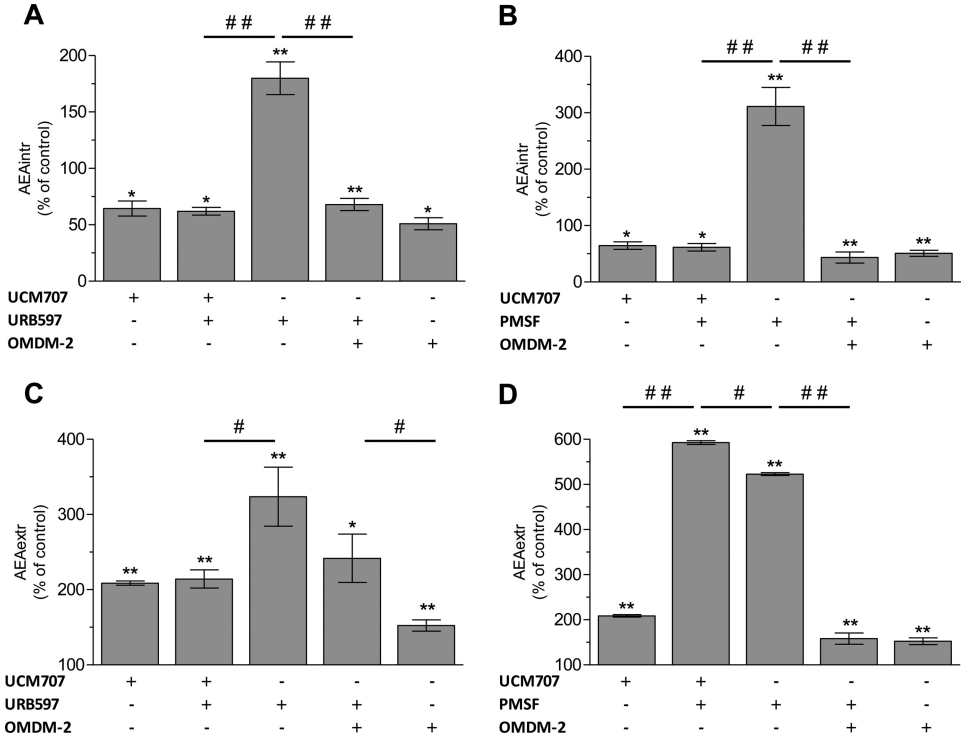

FIGURE 4. **Cellular and extracellular AEA levels measured by GC/MS in the presence of FAAH inhibitors alone or in combination with UCM707 or OMDM-2.** *A*, intracellular AEA level measured after a 5-min incubation of 100 nM AEA and 20-min pretreatment with 100 nM URB597 alone and in the presence of 1 μM UCM707 or 5 μM OMDM-2 in U937 cells (10^6 cells). *B*, the same experiments were carried out in the presence of 1 μM PMSF. In both cases, the intracellular accumulation of AEA induced by URB597 and PMSF was completely abolished in the presence of an EMT inhibitor. In the same experimental conditions, the extracellular AEA accumulation was measured after pretreatment with URB597 alone and in the presence of 1 μM UCM707 or 5 μM OMDM-2 (*C*) or with PMSF alone and in combination (*D*). The values are expressed as a percentage of cellular or extracellular AEA level as compared with vehicle-treated control. Data show mean values ± S.E. (*error bars*) of three independent experiments, each one carried out at least in triplicate. *, $p < 0.05$; **, $p < 0.01$, treated *versus* vehicle-treated control. #, $p < 0.05$; ##, $p < 0.01$, combination treatment *versus* URB597 or PMSF alone.

ronment, and it needs carrier proteins in order to be shuttled from the cell membrane to its intracellular targets (60). The existence of such carriers has been suggested several years ago (32), but only recently different AEA intracellular binding proteins (AIBPs) (60) have been identified, such as FLAT, albumin, Hsp70, and FABP5 and -7 (10, 11, 61). It has also been proposed by Kaczocha *et al.* (9, 61) that FABPs may be the actual target of the EMT inhibitors, which would provide evidence against an membrane protein target. Therefore, we performed experiments using two different cell types that either express or do not express the FABPs endogenously. A recent publication described in detail the U937 proteome, showing a negligible expression of FABPs (44). When U937 cells were differentiated into macrophage-like cells, a dramatic increase of FABP expression levels was shown (44). Making use of this finding, we assessed the effects of UCM707 or OMDM-2 in U937 monocytes and U937 macrophages. As shown in Fig. 5, *A* and *B* (and Fig. 2, *A* and *B*), both UCM707 and OMDM-2 induced an identical concentration-dependent AEA uptake inhibition and extracellular accumulation in both cell types, indicating that these compounds exert their activity independently from the expression of FABPs. Interestingly, unlike in U937 cells, in U937 macrophages, both inhibitors at concentrations higher than 10 μM did not further reduce the cellular uptake. This could be due to the fact that higher concentrations of the UCM707 or OMDM-2 partially inhibit FAAH activity as we observed in our pig brain and cell homogenate experiments (data not shown). As shown above (see Fig. 1, *E* and *F*, and Table 1), U937 macrophages exhibit a negligible incorporation of [^{3}H]ethanolamine, leading to a significantly distinct base-line radioactivity in vehicle-treated cells (~10 times lower in the U937 macrophages). To confirm this, we also tested the effect of URB597 on AEA uptake in U937 cells and U937 macrophages. The results exhibited the same concentration-dependent inhibition of ethanolamine formation, and the extracellular accumulation of [^{3}H]AEA increased in both cell types (Figs. 2*C* and 5*C*). On the other hand, URB597 induced a significant intracellular accumulation of [^{3}H]AEA in macrophages, unlike in U937 cells, where it led to a strong reduction (Figs. 2*C* and 5*C*). In agreement with the differential fate of [^{3}H]ethanolamine in these cell types, we conclude that in U937 macrophages, UCM707 and OMDM-2, at concentrations higher than 10 μM, partially inhibit FAAH, leading to a slight accumulation of intracellular [^{3}H]AEA. The inhibition of EMT and FAAH may contrast with each other, blunting the overall AEA uptake inhibition induced by these AEA transport inhibitors at higher concentrations.

It was reported that by using the specific FAPB inhibitor BMS309403, the AEA uptake was partially inhibited, supporting a crucial role of FABPs in AEA trafficking and breakdown (9). We thus evaluated the effect of BMS309403 in both U937 cells and U937 macrophages. The results shown in Fig. 5*D* reveal no inhibition of [^{3}H]AEA uptake in U937 cells up to 3 μM, a concentration that is 10–100 times higher than the K_i

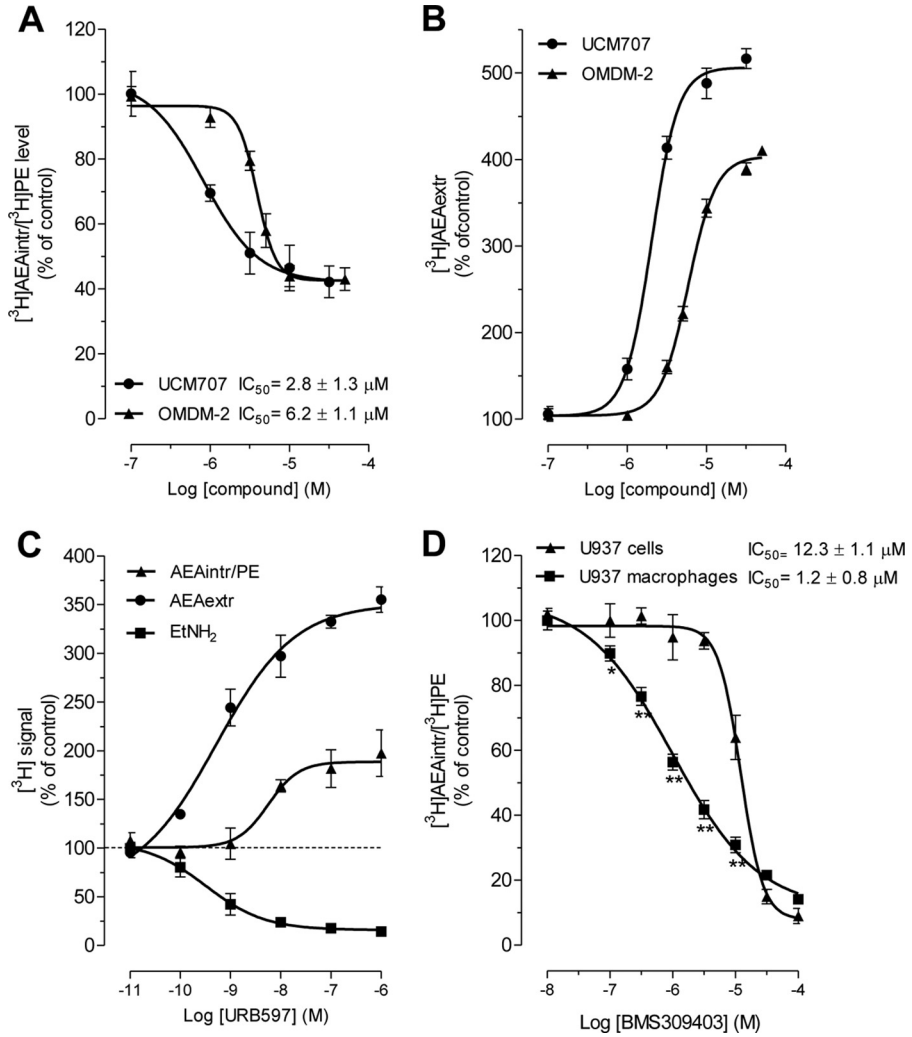

FIGURE 5. **Concentration-dependent [^{3}H]AEA uptake inhibition and extracellular accumulation induced by different inhibitors in U937 macrophages.** Shown are intracellular [^{3}H]AEA uptake inhibition (*A*) and extracellular [^{3}H]AEA accumulation (*B*) measured after a 5-min incubation of 100 nM [^{3}H]AEA plus AEA and 20-min pretreatment with UCM707 or OMDM-2 in U937 macrophages (10^6 cells). The IC_{50} values were calculated from the [^{3}H]AEA uptake inhibition curve. *C*, the same experiments were carried out by pretreating U937 macrophages with different concentrations of URB597. *D*, the concentration-dependent cellular [^{3}H]AEA uptake inhibition induced by the FABP inhibitor BMS309403 was measured in U937 cells and U937 macrophages. The IC_{50} values of BMS309403 calculated for the two cell types are reported in the graph. *, $p < 0.05$; **, $p < 0.01$ intracellular [^{3}H]AEA level in U937 macrophages *versus* U937 cells. *Error bars*, S.E.

values of BMS309403 determined for the different FAPBs (FABP-3, -4, and -5) (62). Conversely, BMS309403 inhibited [^{3}H]AEA uptake in U937 macrophages already at significantly lower concentrations (100–300 nM), in agreement with its K_i value for FABPs (Fig. 5*D*). In keeping with this observation, the calculated IC_{50} value for [^{3}H]AEA uptake by BMS309403 in U937 cells was 10 times higher than in U937 macrophages (12.3 ± 1.1 *versus* 1.2 ± 0.8 μM) (Fig. 5*D*).

Endocannabinoids with an Arachidonoyl Chain Are Transported via the Same Putative EMT but Not Other N-Acylethanolamines—In contrast to the efforts made to elucidate the mechanism of AEA cellular uptake (for reviews, see Refs. 12 and 63), the movement of 2-AG across the cell membrane has only been investigated marginally. Few papers address the issue of 2-AG transport, conveying different hypotheses, from simple diffusion to carrier-mediated transport by the same EMT proposed for AEA or via a different transporter (30–33, 39, 64). Therefore, here we also investigated the cellular uptake of 2-AG, applying the above described methodology.

100 nM AEA plus [^{3}H]AEA was co-incubated with increasing concentrations of 2-AG (generating different ratios between the two endocannabinoids) in U937 cells, leading to a competitive inhibition of [^{3}H]AEA uptake with an IC_{50} of 1.2 ± 0.6 μM (Fig. 6*A*). Accordingly, 2-AG induced a strong concentration-dependent extracellular [^{3}H]AEA accumulation (Fig. 6*A*). The same experiments were carried out by adding 2-AG in presence of 100 nM AEA, and the absolute intracellular and extracellular levels of the latter molecule were quantified by GC/MS. As shown in Fig. 6*B*, 2-AG inhibited the cell membrane movement of AEA in the same qualitative and quantitative manner as observed in the radioactivity-based experiments. At 1 μM, 2-AG led to ~50% inhibition of AEA uptake (Fig. 6*B*).

The same co-incubation experiments were performed, applying different concentrations of AEA in presence of 1 μM of either 2-AG or 2-AG/[^{3}H]2-AG. In Fig. 6*C*, the AEA-

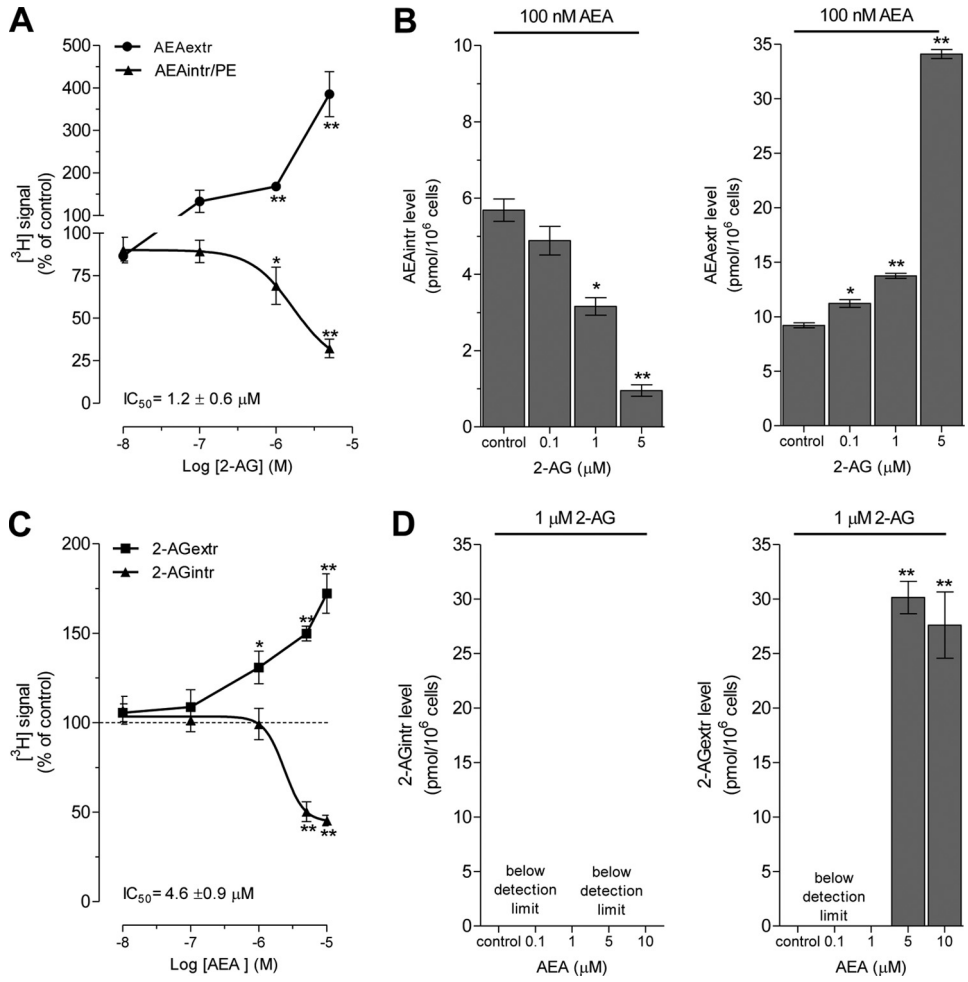

FIGURE 6. **AEA and 2-AG competition for the cellular uptake in U937 cells.** *A*, concentration-dependent cellular [^{3}H]AEA uptake inhibition and extracellular [^{3}H]AEA accumulation after 5-min incubation of 100 nM [^{3}H]AEA plus AEA in the presence of different concentrations of 2-AG (0.01–5 μM) in U937 cells (10^6 cells). *B*, intracellular and extracellular AEA levels measured by CG/MS after a 5-min incubation with 100 nM AEA in the presence of different concentrations of 2-AG (0.1–5 μM) in U937 cells (10^6 cells). *C*, concentration-dependent cellular [^{3}H]2-AG uptake inhibition and extracellular [^{3}H]2-AG accumulation after a 5-min incubation of 1 μM [^{3}H]2-AG plus 2-AG in the presence of different concentrations of AEA (0.01–10 μM) in U937 cells. *D*, intracellular and extracellular 2-AG levels measured by CG/MS after a 5-min incubation with 1 μM 2-AG in the presence of 0.1–10 μM AEA in U937 cells (10^6 cells). The values are expressed as a percentage of cellular and extracellular [^{3}H]AEA or [^{3}H]2-AG levels as compared with vehicle-treated control. For the absolute endocannabinoid quantification, the values are expressed as pmol of AEA or 2-AG/10^6 cells. Data show mean values ± S.E. (*error bars*) of three independent experiments, each one carried out at least in triplicate. *, $p < 0.05$; **, $p < 0.01$, treated *versus* vehicle-treated control.

mediated inhibition of [^{3}H]2-AG uptake is shown with an IC_{50} value of 4.9 ± 0.9 μM. In the same graph, the AEA-induced extracellular accumulation of [^{3}H]2-AG is also shown. In agreement with the kinetic experiments mentioned above, the intracellular 2-AG level measured by GC/MS was below the limit of detection both in vehicle-treated and AEA-co-incubated cells. At higher AEA concentrations, the extracellular level of 2-AG became detectable, whereas it was not measurable in the vehicle-treated cells (Fig. 6*D*). Collectively, these data show a competition between the two endocannabinoids for the same membrane carrier. In all of the other conditions tested, the intracellular and extracellular levels of 2-AG were too low to be detected, probably due to the multienzymatic pathways involved in 2-AG hydrolytic cleavage as well as the higher detection limit of 2-AG compared with AEA (50).

We recently established a method to quantify the levels of other endogenous *N*-acylethanolamines, such as PEA, OEA, SEA, and LEA, by GC/MS (50). We applied this method to investigate the AEA and 2-AG uptake in the presence of these *N*-acylethanolamines. As shown in Fig. 7, neither AEA nor 2-AG cellular uptake was influenced by the presence of these *N*-acylethanolamines. This suggests that the latter lipids are not transported via the putative EMT (Fig. 7), which is in agreement with two studies showing a lack of competition between AEA and PEA (65) and between AEA or 2-AG and SEA (66). The absolute intracellular and extracellular levels of all *N*-acylethanolamines were quantified upon administration to the cells, either alone or together, because the latter condition more closely resembles the physiological conditions. All of the *N*-acylethanolamines exhibited an increase of both the intracellular and extracellular levels when administered simultaneously in comparison with the single administration. Nonetheless, the intra-/extracellular ratio did not exhibit any change (Fig. 7), suggesting that the FAAH hydrolysis rather than the movement across the cell membrane is affected. All of these fatty acid-derived *N*-acylethanolamines are FAAH substrates and can compete for the enzymatic hydrolysis. Again, 2-AG was

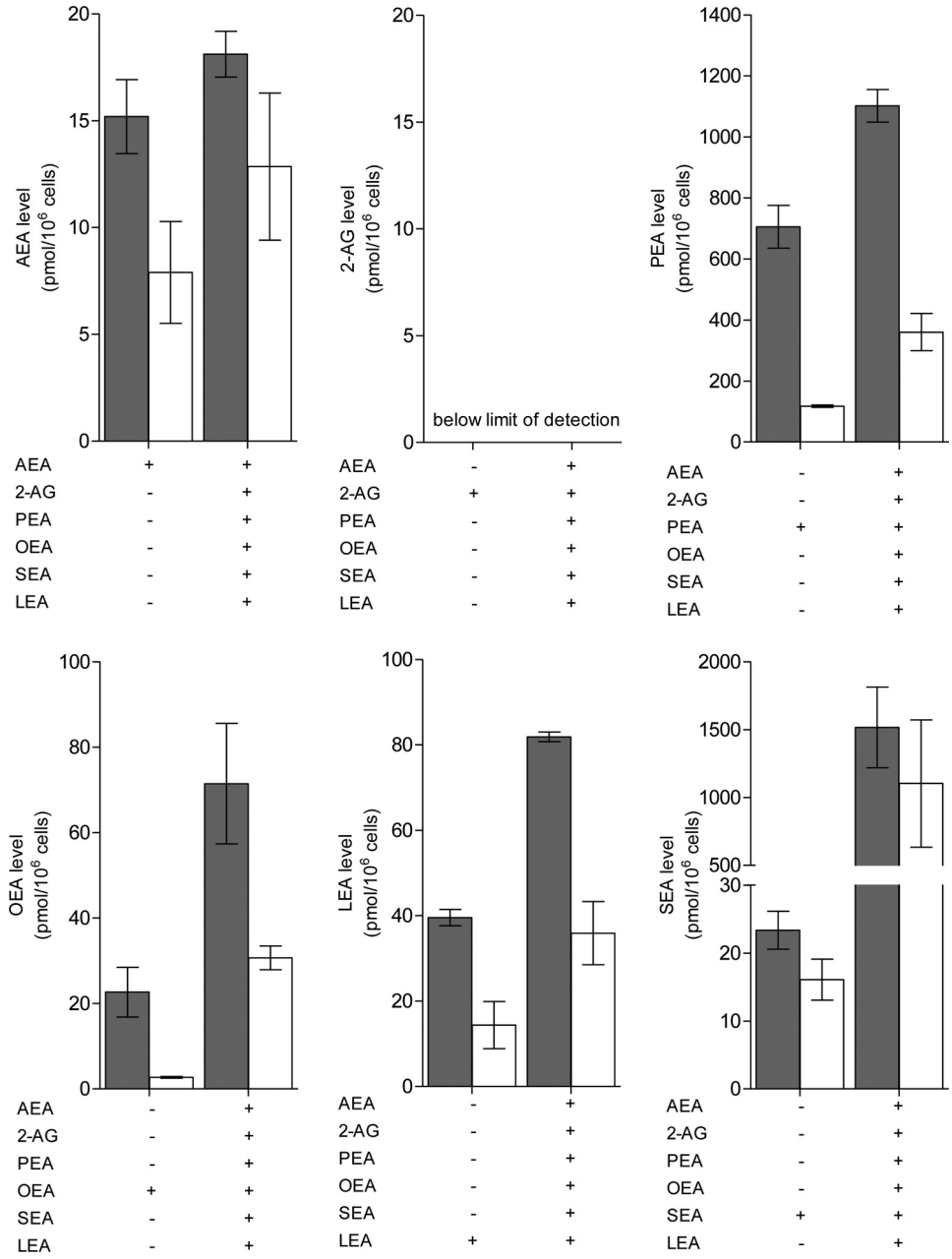

FIGURE 7. **Other *N*-acylethanolamines do not compete with AEA and 2-AG for the cellular uptake in U937 cells.** Shown are intracellular (*gray bars*) and extracellular (*white bars*) AEA, 2-AG, PEA, OEA, LEA, and SEA levels measured (by GC/MS) alone or in combination after a 5-min incubation of 100 nM AEA and/or 1 μM 2-AG and/or 1 μM PEA and/or 100 nM OEA and/or 100 nM LEA and/or 100 nM SEA in U937 cells (10^6 cells). The levels of 2-AG were below the limit of detection. The values are expressed as pmol of compound/10^6 cells. Data show mean values ± S.E. (*error bars*) of three independent experiments, each one carried out at least in triplicate.

not measurable as in the experiments shown in Fig. 6*D* (100 nM AEA).

To further explore the structural requirements of lipids that are transported via the same mechanism as AEA and 2-AG, we next measured whether other arachidonic acid-derived endocannabinoids affect [^{3}H]AEA and [^{3}H]2-AG transport. As shown in Fig. 8, *A–C*, NADA, virodhamine, and 2-AGE all competed with the uptake of both [^{3}H]AEA and [^{3}H]2-AG with similar potencies, reducing their intracellular levels and increasing their extracellular levels. Intriguingly, this competition occurred independently of the inhibition of enzymatic hydrolysis of the major endocannabinoids, as shown by the fact that all endocannabinoids inhibit both [^{3}H]AEA and [^{3}H]2-AG cellular uptake, irrespective of their FAAH and MAGL inhibition activity (for MAGL inhibition, see also below). We used PEA as a control to see the FAAH inhibition in this setup (Fig. 8*D*). As expected, 10 μM PEA did not affect [^{3}H]2-AG uptake and hydrolysis but significantly reduced [^{3}H]AEA cellular uptake and hydrolysis by about 50%.

Intracellular 2-AG Accumulation Induced by JZL184 Is Inhibited by EMT Inhibitors in U937 Cells—The effect of AEA cellular uptake inhibitors was also investigated upon 2-AG cellular uptake. Figs. 9, *A* and *B*, shows the concentration-dependent inhibition of [^{3}H]2-AG uptake induced by UCM707 and

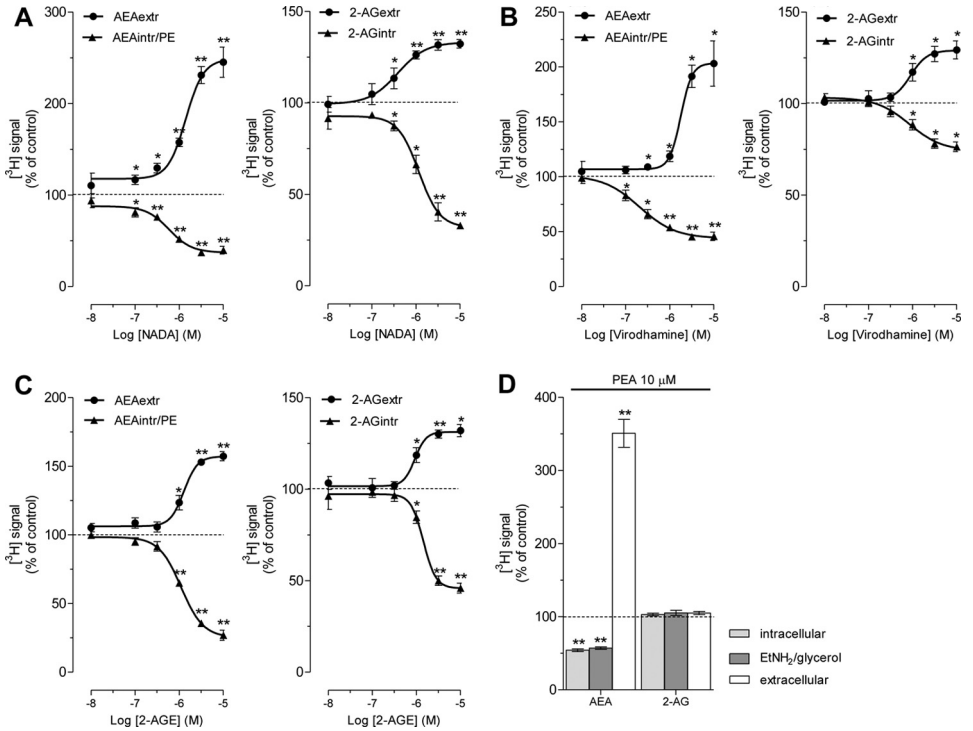

FIGURE 8. **All endocannabinoids compete with AEA and 2-AG for the cellular uptake in U937 cells.** Shown are concentration-dependent cellular [^{3}H]AEA or [^{3}H]2-AG uptake inhibition and extracellular [^{3}H]AEA or [^{3}H]2-AG accumulation after a 5-min incubation of 100 nM [^{3}H]AEA plus AEA or 1 μM [^{3}H]2-AG plus 2-AG in the presence of different concentrations of NADA (*A*), virodhamine (*B*), and noladin ether (*2-AGE*) (*C*) in U937 cells (10^6 cells). *D*, intracellular and extracellular [^{3}H]AEA or [^{3}H]2-AG levels and [^{3}H]$EtNH_2$ or [^{3}H]glycerol levels after a 5-min incubation of 100 nM [^{3}H]AEA plus AEA or 1 μM [^{3}H]2-AG plus 2-AG in the presence of 10 μM PEA in U937 cells. The values are expressed as a percentage of cellular and extracellular [^{3}H]AEA or [^{3}H]2-AG levels and [^{3}H]$EtNH_2$ or [^{3}H]glycerol levels as compared with vehicle-treated control. Data show mean values ± S.E. (*error bars*) of three independent experiments, each one carried out at least in triplicate. *, $p < 0.05$; **, $p < 0.01$, treated *versus* vehicle-treated control.

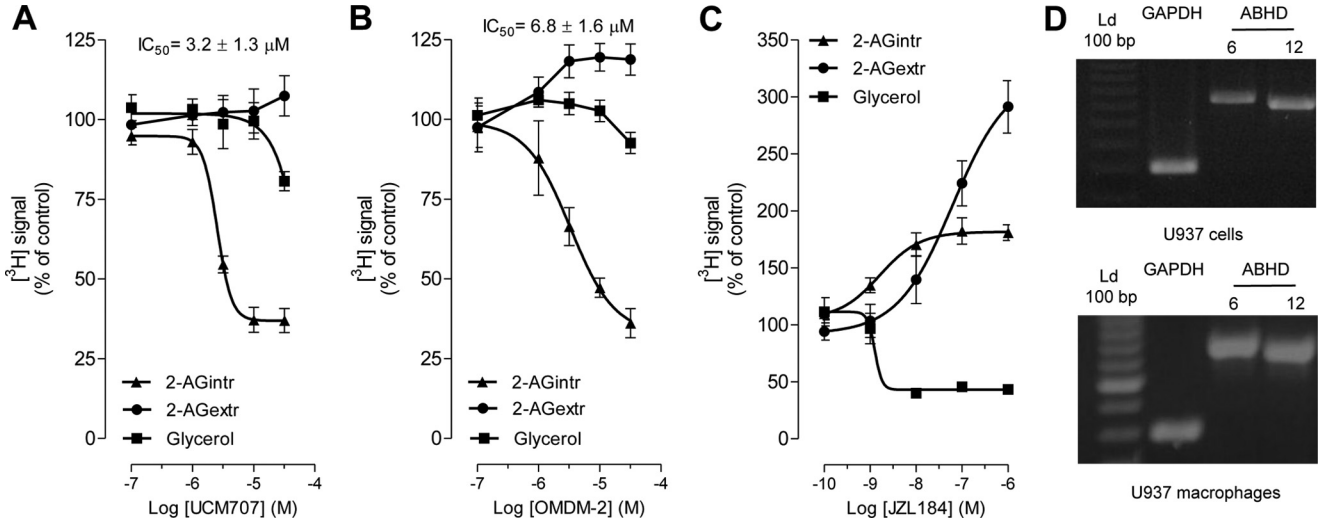

FIGURE 9. **Concentration-dependent [^{3}H]2-AG uptake inhibition and extracellular accumulation induced by UCM707, OMDM-2, and JZL184 in U937 cells.** Shown are concentration-dependent cellular [^{3}H]2-AG, extracellular [^{3}H]2-AG, and [^{3}H]glycerol levels after a 5-min incubation of 1 μM [^{3}H]2-AG plus 2-AG in the presence of different concentrations of UCM707 (*A*), OMDM-2 (*B*), and JZL184 (*C*) in U937 cells (10^6 cells). The values are expressed as a percentage of cellular and extracellular [^{3}H]2-AG level and [^{3}H]glycerol level as compared with vehicle-treated control. The radioactive signal for [^{3}H]glycerol represents the sum of the radioactivity recovered in the aqueous phases coming from cell and supernatant. Data show mean values ± S.E. (*error bars*). of three independent experiments, each one carried out at least in triplicate. *D*, RT-PCR characterization of ABHD expression in U937 cells (*top*) and U937 macrophages (*bottom*). Total RNA was extracted from 5×10^6 cells, and mRNA expression was examined by RT-PCR. The expected sizes of the RT-PCR products are 300 bp for GAPHD, 673 bp for ABHD-6, and 638 bp for ABHD-12.

OMDM-2 treatment, with the same potency as observed for the [^{3}H]AEA cellular uptake. The IC_{50} values were 3.2 ± 1.3 and 6.8 ± 1.1 μM for UCM707 and OMDM-2, respectively, whereas for AEA uptake, the values were 1.8 ± 0.8 and 5.2 ± 0.9 μM (Figs. 2 (*A* and *B*) and 9 (*A* and *B*)). Unexpectedly, unlike with AEA, the treatment with UCM707 and OMDM-2 did not lead to a significant concentration-dependent increase of the extracellular [^{3}H]2-AG level and a reduction of the hydrolytic byproduct [^{3}H]glycerol (Fig. 9, *A* and *B*). In order to determine the contribution of 2-AG hydrolysis in the 2-AG uptake, U937

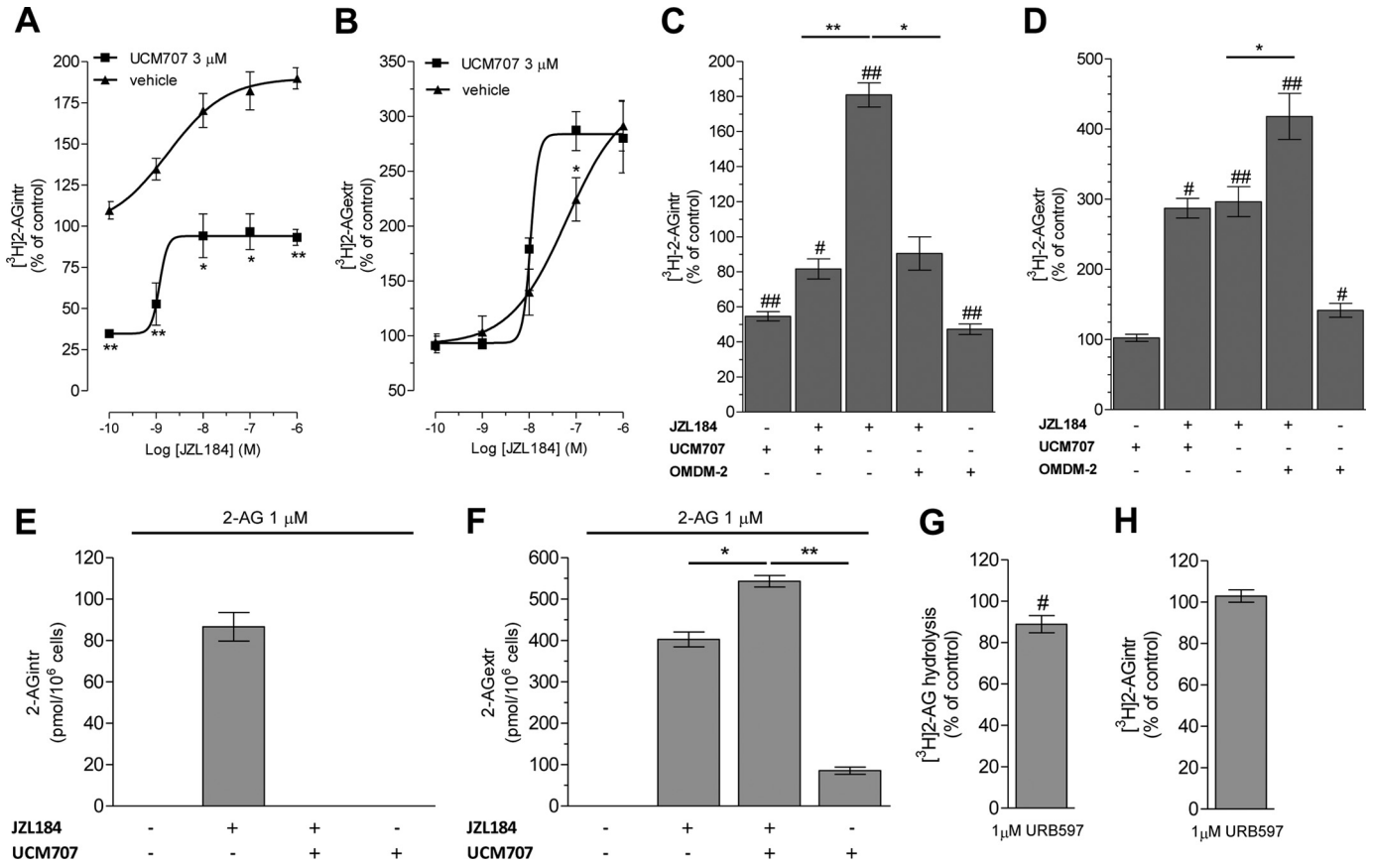

FIGURE 10. **Concentration-dependent [^{3}H]2-AG uptake accumulation induced by JZL184 alone or in combination with 3 μM UCM707.** *A*, concentration-dependent cellular [^{3}H]2-AG uptake inhibition after a 5-min incubation of 1 μM [^{3}H]2-AG plus 2-AG and 20-min pretreatment with JZL184 alone and in the presence of 3 μM UCM707 in U937 cells (10^6 cells). *B*, the concentration-dependent extracellular [^{3}H]2-AG accumulation measured in the same experimental conditions is shown for JZL184 alone or in the presence of 3 μM UCM707. Shown are cellular [^{3}H]2-AG uptake inhibition (*C*) and extracellular [^{3}H]2-AG accumulation (*D*) after a 5-min incubation with 1 μM [^{3}H]2-AG plus 2-AG and 20-min pretreatment with 1 μM UCM707, 5 μM OMDM-2, and 1 μM JZL184 alone or in combinations in U937 cells. Shown are intracellular (*E*) and extracellular (*F*) 2-AG levels measured (by GC/MS) after a 5-min incubation of 1 μM 2-AG and a 20-min pretreatment with 1 μM JZL184 and 3 μM UCM707 alone or in combination in U937 cells. Shown are [^{3}H]2-AG hydrolysis (measured in U937 cell homogenate) (*G*) and cellular [^{3}H]2-AG uptake (measured in U937 cells) (*H*) in the presence of 1 μM URB597. The values are expressed as a percentage of cellular or extracellular [^{3}H]2-AG level as compared with vehicle-treated control. For the absolute 2-AG quantification, the values are expressed as pmol/10^6 cells. Data show mean values ± S.E. (*error bars*) of three independent experiments, each one carried out at least in triplicate. #, $p < 0.05$; ##, $p < 0.01$ *versus* control. *, $p < 0.05$; **, $p < 0.01$ combination treatment *versus* JZL184 alone.

cells were treated with increasing concentrations of JZL184, a specific MAGL inhibitor, which resulted in a significant increase of both intracellular and extracellular [^{3}H]2-AG levels as well as a reduction of the [^{3}H]glycerol formation (Fig. 9*C*). As mentioned above, enzymes other than MAGL are involved in 2-AG breakdown, and therefore the selective blockage of MAGL resulted only in a partial reduction (55%) of [^{3}H]glycerol formation as compared with the vehicle-treated cells. The residual 2-AG hydrolysis mainly depends on ABHD-6 and -12; in fact, the multiple inhibition of MAGL (by 1 μM JZL184), ABHD-6 (WWL70, 10 μM), and ABHD-12 (tetrahydrolipstatin, 20 μM) led to an 80%–85% inhibition of 2-AG hydrolysis in U937 cell homogenate (data not shown). Moreover, U937 cells and U937 macrophages showed robust mRNA expression levels of both ABHD-6 and ABHD-12 (Fig. 9*D*). In subsequent experiments, we combined 3 μM UCM707 with increasing concentrations of JZL184 (0.1–1000 nM), as performed previously with AEA. As shown in Fig. 10*A*, the combination treatment reversed the intracellular accumulation of [^{3}H]2-AG mediated by JZL184, resulting in a significant reduction of the intracellular endocannabinoid level. The extracellular level was not significantly increased in the presence of the combination as compared with the JZL184 treatment alone (Fig. 10*B*). This lack of potentiation for the combination is in line with the negligible effect induced by 3 μM UCM707 (≅105% of control) on extracellular [^{3}H]2-AG accumulation (see Fig. 9*A*). The combination treatment was also carried out with the EMT inhibitor OMDM-2 at 5 μM combined with 1 μM JZL184. As shown for UCM707, the OMDM-2/JZL184 combination induced a significant reduction of the intracellular [^{3}H]2-AG accumulation as compared with JZL184 treatment alone. Unlike with UCM707, the combination of JZL184 with OMDM-2 led to a slight but significant increase of the extracellular endocannabinoid level. Although not understood at present, this is in agreement with the slight increase (about 25%) of the extracellular [^{3}H]2-AG induced by 5 μM OMDM-2 alone (Fig. 10, *C* and *D*).

Likewise, the combination of UCM707 and JZL184 abolished the absolute intracellular amount of 2-AG seen with GC/MS upon JZL184 treatment (80 pmol/10^6 cells). In the vehicle-treated cells and the UCM707 treated cells, the 2-AG level was below the limit of detection (Fig. 10*E*). The UCM707/JZL184

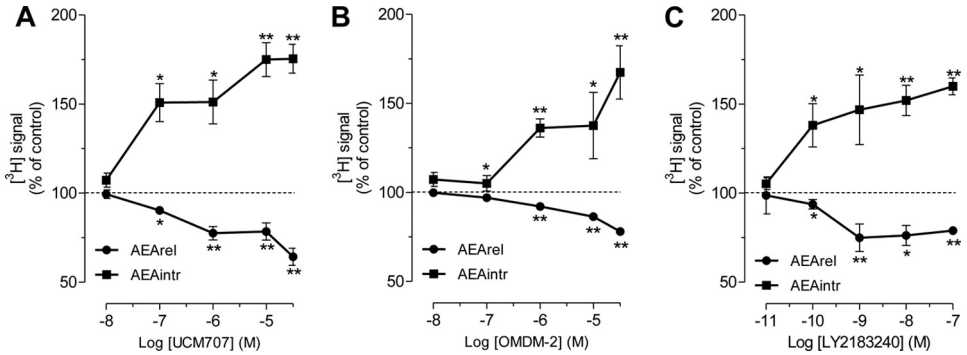

FIGURE 11. **EMT inhibitors block [^{3}H]AEA release from U937 cells preloaded with 100 nM [^{3}H]AEA plus AEA.** Shown are concentration-dependent intracellular [^{3}H]AEA (*AEAintr*) accumulation and extracellular [^{3}H]AEA released (*AEArel*) reduction after a 25-min incubation of UCM707 (*A*), OMDM-2 (*B*), or LY2183240 (*C*) in FAAH-blocked U937 cells (obtained by cellular pretreatment with 100 nM URB597 and 1 μM PMSF) preloaded with 100 nM [^{3}H]AEA plus AEA. The values are expressed as a percentage of cellular or extracellular [^{3}H]AEA levels as compared with vehicle-treated control. Data show mean values $\pm$ S.E. (*error bars*) of three independent experiments, each one carried out at least in triplicate. *, $p < 0.05$; **, $p < 0.01$, treated *versus* vehicle-treated control.

combination treatment also led to a slight but significant increase of the extracellular 2-AG over the increase observed with JZL184 alone (500 pmol *versus* 400 pmol/10^6 cells (Fig. 10*F*). FAAH activity does not significantly contribute to the [^{3}H]2-AG hydrolysis (assessed in U937 cell homogenate) (Fig. 10*G*) and cellular uptake into U937 cells (Fig. 10*H*), as shown by blocking FAAH with 1 μM URB597.

The Putative EMT Mediates a Bidirectional Transport of AEA and 2-AG in U937 Cells—The release (efflux) mechanism of endocannabinoids is still unknown, and very few studies have addressed this issue only for AEA (16, 37–39). In order to investigate the hypothesis that the same EMT is involved in both the release and uptake, we adapted a method to indirectly load the cells with [^{3}H]AEA or [^{3}H]2-AG (see "Experimental Procedures"). In this system, we achieved an almost complete pharmacological inhibition of endocannabinoid breakdown by using a combination of URB597 and PMSF (FAAH) or by using JZL184 (MAGL), tetrahydrolipstatin, and WWL70 (ABHD-6 and -12). Subsequent to inhibition of hydrolysis, cells were incubated with a mixture of "cold/hot" endocannabinoids, which accumulated intracellularly as shown before, despite the lack of the gradient generated by continuous breakdown. Afterward, the EMT inhibitors UCM707, OMDM-2, and LY2183240 were applied, and the extracellular release of the preloaded [^{3}H]AEA or [^{3}H]2-AG was measured after 25 min of incubation in an endocannabinoid-free medium containing 1% fatty acid-free BSA as an extracellular "acceptor." As shown in Fig. 11, *A–C*, all three EMT inhibitors significantly inhibited the [^{3}H]AEA release in a concentration-dependent manner. As expected, the EMT inhibitor-treated cells also revealed a strong increase of the cytosolic [^{3}H]AEA level. In agreement with the cellular release of [^{3}H]AEA shown, all three EMT inhibitors also partially inhibited the release of [^{3}H]2-AG and increased its intracellular level in a concentration-dependent manner (Fig. 12, *A–C*). Importantly, all three EMT inhibitors showed a similar potency and efficacy in inhibiting the release of both endocannabinoids. Collectively, these results show, for the first time, that the putative EMT, as characterized by its inhibitors, is involved in the bidirectional movement of AEA and 2-AG.

DISCUSSION

Endocannabinoids have been shown to be involved in numerous physiological and pathophysiological processes (1). Their generation, transport, and degradation are fundamental for the functioning of the ECS. The mechanism of endocannabinoid movement across the cell membrane is a controversial issue, despite almost 2 decades of research activity on this topic. There are both *in vitro* (12, 63) and *in vivo* (67–70) data supporting the existence of a putative anandamide EMT. However, other EMT-independent AEA uptake mechanisms have been proposed, such as caveolae-related endocytosis (27, 71) and FAAH-driven facilitated diffusion (24, 25, 72). More recently, different cytoplasmic AEA-binding proteins (FABPs, Hsp70, albumin, and FLAT) and intracellular compartments (adiposomes) have been shown to be important for the cellular uptake of AEA (9, 11, 60, 73). Because the methodology used in endocannabinoid cellular transport assays is fundamental for the interpretation of the data obtained, as previously pointed out (40, 41), we have made use of absolute quantifications of endocannabinoids in addition to radioligand assays (see below). All of our experiments were carried out without serum in order to avoid any alteration of the actual extracellular concentration of AEA and 2-AG (50). By using silanized plastic tubes (see "Experimental Procedures"), we were able to overcome the inherent problem of AEA and 2-AG sticking to plastic, as previously described (40, 41), and the total recovery of AEA and 2-AG (sum of extracellular and intracellular endocannabinoids and their hydrolytic products) at the end of the experiments was always in the range of 85–95% of the initial amount added to the cells (data not shown).

Distinct Incorporation of [^{3}H]Ethanolamine and [^{3}H]Glycerol into U937 Cell Membranes and Implications for Uptake Assays—Current methodologies applied to investigate endocannabinoid cell membrane transport mainly rely on the measurement of radiolabeled AEA, detecting the intra- and extracellular radioactive signal after a lipophilic/aqueous phase separation. Consequently, the position of the radioisotope in the endocannabinoid critically affects the readout. Indeed, after hydrolysis, the free arachidonate and the PL-incorporated arachidonic acid are collected within the lipophilic phase,

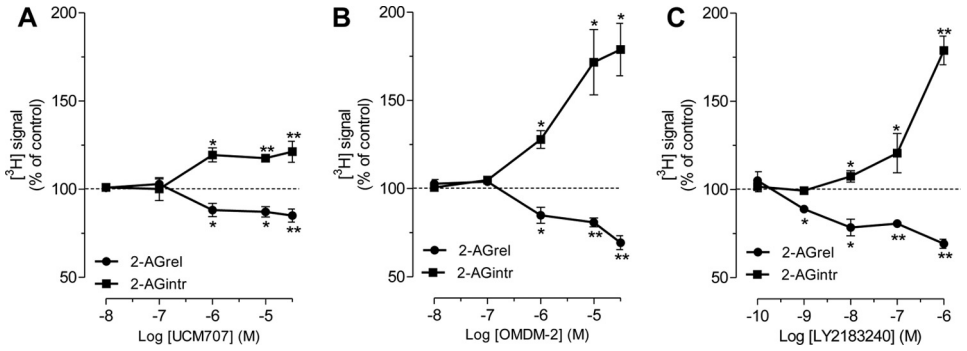

FIGURE 12. **EMT inhibitors inhibit [^{3}H]2-AG release from U937 cells preloaded with 1 μM [^{3}H]2-AG plus 2-AG.** Shown are concentration-dependent intracellular [^{3}H]2-AG (*2-AGintr*) accumulation and extracellular [^{3}H]2-AG released (*2-AGrel*) reduction after a 25-min incubation with UCM707 (*A*), OMDM-2 (*B*), or LY2183240 (*C*) in MAGL-, ABHD-6-, and ABHD-12-blocked U937 cells (obtained by cellular pretreatment with 1 μM JZL184, 10 μM WWL70, and 20 μM tetrahydrolipstatin) preloaded with 1 μM [^{3}H]2-AG plus 2-AG. The values are expressed as a percentage of cellular or extracellular [^{3}H]2-AG levels as compared with vehicle-treated control. Data show mean values ± S.E. (*error bars*) of three independent experiments, each one carried out at least in triplicate. *, $p < 0.05$; **, $p < 0.01$, treated *versus* vehicle-treated control.

whereas the ethanolamine (or glycerol from 2-AG) is recovered in the aqueous phase. Therefore, when [*ethanolamine*-1-^{3}H]AEA is used in the presence of either FAAH or EMT inhibitors, the intracellular radioactivity from the lipophilic phase should be differentially affected. FAAH inhibition leads to higher intracellular levels of AEA compared with vehicle-treated cells, as reported for URB597 (56, 74, 75), whereas blocking the cell membrane transport leads to a reduced cellular penetration of AEA, as reported for several inhibitors (19–21). FAAH inhibitors can lead to different readouts, depending on many factors, such as AEA concentration, distinct incorporation of ethanolamine in different cell types, and method of detection (radioactivity *versus* absolute quantification). This could be a major explanation for the different readouts reported for FAAH inhibitors on AEA cellular uptake (25, 56, 74, 76). If FAAH is blocked, AEA is still transported inside the cell, where it segregates into cytoplasmic reservoirs, such as the recently described carrier proteins or adiposomes (9–11, 73), whereas in FAAH-active cells, AEA is rapidly hydrolyzed. Selective EMT inhibitors inhibit AEA uptake without significantly interfering with the enzymes involved in endocannabinoid degradation (Refs. 19 and 20 and this work). In our experiments, we incubated U937 cells with [*ethanolamine*-1-^{3}H]AEA, finding a similar reduction of the cytosolic radioactivity signal by pretreating the cells with either URB597, PMSF, or OMDM-2 and UCM707. On the contrary, when the same experiments were carried out measuring the absolute intra- and extracellular endocannabinoid levels in a radiolabel-free assay, the EMT inhibition led to a decreased cytoplasmic AEA level, whereas inhibition of FAAH led to intracellular accumulation. The discrepancy between the two experimental settings was explained upon performing TLC analyses, showing that PE-incorporated [^{3}H]ethanolamine is the major source (74.9%) of the intracellular radioactivity signal in the vehicle-treated cells. Importantly, this leads to an overestimation of the cytoplasmic [^{3}H]AEA level. The arachidonic acid derived from AEA hydrolysis was shown to be almost completely incorporated into PLs in both rodent cancer cells and primary cortical neurons (17, 18), whereas on the contrary, the ethanolamine was not found in PLs after 5 min of incubation with [^{3}H]AEA in RBL-2H3 rat basophilic leukemia cells (25) or only partially incorporated into primary cortical rat neurons (17). Ethanolamine is involved in different cellular processes, and it is essential for biosynthesis of the most abundant phospholipids, phosphatidylcholine and phosphatidylethanolamine (77). The ethanolamine PL incorporation is a well known multistep pathway (see supplemental Fig. 1) that initiates with the ethanolamine phosphorylation, catalyzed by choline or ethanolamine kinases, two soluble cytoplasmic enzymes. Subsequently, phosphoethanolamine reacts with CTP to generate CDP-ethanolamine, which in turn is condensed with 1,2-diacylglycerol to produce PE via the enzymatic activity of the ER-expressed CDP-ethanolamine:diacylglycerol ethanolamine phosphotransferase (78). AEA hydrolysis occurs mainly at the ER level, where FAAH is primarily expressed and where the rate-limiting step of the PE biosynthesis takes place. AEA-generated [^{3}H]ethanolamine is included in the cytosolic pool of ethanolamine and fed to the PL biosynthesis. This constitutive incorporation of [^{3}H]ethanolamine can directly impact the readout of the [^{3}H]AEA uptake assay. Although a former study ruled out a significant PL incorporation of [^{3}H]ethanolamine in RBL-2H3 (25), most of the studies on AEA uptake have been performed using cancer cell lines that have been shown to possess a high activity of the PL biosynthesis pathway due their rapid and unlimited proliferation rate (18). In fact, choline kinase has been reported to be overexpressed in many cancer types, where it promotes proliferation (79). In the present study, we show that the human U937 monocyte leukemia cells retain the vast majority of the AEA-derived [^{3}H]ethanolamine in PLs within 5 min due to the high rate of PL biosynthesis in this cell line (80). Importantly, the non-proliferating PMA-differentiated U937 macrophages negligibly incorporate ethanolamine. Similarly, RBL-2H3 cells probably possess a lower rate of PLs biosynthesis, which would explain the difference observed in ethanolamine incorporation. Unlike ethanolamine, [^{3}H]glycerol generated upon 2-AG hydrolysis has a different intracellular fate because it is only poorly incorporated into PLs (0.2%). Glycerol is the backbone of glycerophospholipids, the most abundant class of lipids in mammalian cells. Its biosynthesis takes place in the ER, and it is initiated by the acylation of glycerol 3-phosphate to form phosphatidic acid, which represents the common precursor for all of the other glycerophospholipids (77).

[^{3}H]Glycerol formation occurs at the cell membrane, where the 2-AG hydrolytic enzymes MAGL, ABHD-6, and ABHD-12 are located (58, 59). According to the MAGL crystal structure, glycerol can leave the catalytic site via a specific exit channel (81) and freely diffuse throughout the cell membrane, despite its hydrophilic nature. This can happen thanks to the aquaglyceroporins (AQPs), a class of transmembrane water channels, which are also permeable to glycerol (82). Recently, the expression of two aquaglyceroporin members, AQP3 and AQP9, has been identified in macrophages (83, 84). Therefore, [^{3}H]glycerol formed upon 2-AG cleavage is unlikely to enter the intracellular pool available for glycerophospholipid biosynthesis.

Independent Interaction between FAAH Inhibitors and EMT Inhibitors upon AEA Uptake—The main indirect proof for the existence of the EMT was obtained by treating cells with different inhibitors of cellular uptake of AEA at concentrations at which they do not interact with FAAH (19–21). Moreover, in the literature, there is some evidence against the causal relationship between the inhibition of AEA degradation and the inhibition of cellular uptake. Centonze *et al.* (85) showed that two natural products, quinpirole and cocaine, act as FAAH inhibitors in corticostriatal slices without affecting AEA uptake in corticostriatal synaptosomes. Furthermore, inhibition of AEA uptake independent of FAAH inhibition has been reported to produce a variety of *in vivo* effects, including antinociception, in animal models of neuropathic pain (67–70). Here we show that the combination treatment of an EMT inhibitor (UCM707 or OMDM-2) at low and FAAH-ineffective concentrations with the selective FAAH inhibitor URB597 or the nonspecific hydrolase inhibitor PMSF results in a functional synergism on the AEA uptake inhibition, in agreement with an independent interaction between the two classes of inhibitors (46–48). The weak FAAH inhibition by low concentrations of inhibitors could be amplified by increased EMT activity due to CB_1 receptor stimulation. Several papers have suggested a regulatory loop between CB_1 receptors and EMT, where receptor activation triggers a higher EMT activity (86, 87). Maccarrone *et al.* (86) reported a NO-mediated link between CB_1 and EMT in endothelial cells, and Ortega-Gutiérrez *et al.* (87) showed a SR141716A-sensitive contribution of AEA uptake into neuronal cortical cells obtained from both $FAAH^{+/+}$ and $FAAH^{-/-}$ mice. In this study, the increased amount of extracellular AEA triggered by the EMT inhibitors might activate CB_1 receptors, which are expressed on the cell surface of the U937 clone we used (data not shown) (88, 89). FAAH inhibition by the EMT inhibitors can be ruled out because we chose concentrations at which UCM707 (1 μM) and OMDM-2 (5 μM) do not inhibit FAAH (19, 20), which was confirmed by us in two different experiments, including U937 cell homogenate. The results on the combination effects of EMT and FAAH inhibitors, reported here for the first time, show an independent interaction based on the activity on two different targets (*i.e.* FAAH and EMT).

The EMT and Cytoplasmic AEA-binding Proteins Are Different Players in the AEA Uptake Process—Two recent papers have reported the binding of several EMT inhibitors to FAPB5 and FLAT in the micromolar range (11, 61). In addition, UCM707 at 20 μM was shown to inhibit AEA accumulation in FLAT-expressing HEK293 cells (11), whereas OMDM-2 at 10 μM partially reduced AEA uptake in FAAH-transfected HeLa cells, probably competing with AEA for FABP5 binding (61). Although in our experiments we applied these two EMT inhibitors at significantly lower concentrations (5–10 times), a potential weak interaction with FABPs and FLAT (if present in cells) cannot be completely ruled out. Independent groups have identified different intracellular carrier proteins, such as FABPs, FLAT, albumin, and Hsp70, which were collectively named AIBPs (60), which shuttle AEA within the cytosol to different intracellular compartments and targets (9–11, 60, 61). Although AIPBs certainly play an important role in cellular AEA uptake, these recent reports indicate that carrier proteins are crucially involved in the complex AEA trafficking process without ruling out an EMT-mediated uptake step. Indeed, Fu *et al.* (11) showed that FLAT specifically binds AEA and not 2-AG, and Oddi *et al.* (10) reported the same for albumin and Hsp70. However, our data clearly indicate that the cellular uptake process of AEA and 2-AG occurs via the same mechanism. Furthermore, Fu *et al.* (11) described some other intriguing findings in favor of the existence of an EMT. They showed the trend of the EMT inhibitors UCM707 and VDM11 to inhibit AEA uptake in FLAT-transfected HEK293 cells more strongly than in the vector-transfected cells (11). HEK293 cells have been shown to possess the EMT (although with a lower V_{max} value than U937 cells) and almost completely lack FAAH activity (16, 90, 91). Therefore, the additional AEA uptake inhibition by UCM707 and VDM11 in FLAT-transfected cells over mock-transfected cells may be a combination of separate effects on FLAT and EMT. This hypothesis is supported by the inability of the specific FLAT inhibitor ARN272 to produce any additional reduction of AEA uptake in FLAT-transfected cells. Furthermore, the accumulation of intracellular AEA after 5 min of incubation in neurons isolated from FAAH/FLAT-deficient mouse brain is almost half of the AEA level found in neurons isolated from wild type mice, suggesting that these cells exploit other transport mechanisms in addition to FAAH/FLAT for AEA uptake. Finally, Fu *et al.* (11) also identified a role of FLAT in the release of AEA. In the culture medium obtained from Neuro-2a FLAT-transfected cells, a significantly higher amount of AEA was found in vector-transfected cells (11). Importantly, FLAT expression did not induce any effect on 2-AG, whereas we report a role of the EMT in the release of both endocannabinoids. Two recent papers (9, 61) identified different FABPs as intracellular AEA carrier proteins, describing their involvement in the AEA uptake process in both COS-7 transfected cells and the endogenously FABP-expressing HeLa cells (61). Interestingly, the specific FABPs inhibitor BMS309403 has been shown to only partially reduce the AEA uptake in FABP-transfected COS-7 and N18TG2 cells at concentrations higher than 20 and 50 μM, respectively (although the reported K_i is in the nanomolar range (62)). In HeLa cells, both the pharmacological and genetic inhibition of FABPs led to a partial inhibition of the nuclear PPARα activation triggered by OEA and GW747 (two PPAR agonists), thus confirming the intracellular shuttling role of FABPs for these compounds. However, the authors did not show the role of FABPs in AEA-triggered PPARα activation. Furthermore, the authors showed a partial reduction of AEA uptake in FAAH-transfected HeLa

cells that was lost in FABP-deficient cells, which led them to hypothesize that these proteins are the main target of the EMT inhibitors used. In this study, we evaluated the potency of AEA uptake inhibition by UCM707 and OMDM-2 using U937 cells and U937 macrophages, which have recently been shown to differentially express FABPs (44). The authors monitored changes in the proteome in monocyte-like U937 cells and upon stimulation with PMA (macrophage-like phenotype). In U937 macrophages, the levels of FABP5 increase about 4-fold, and FABP4 levels increase dramatically because they are not expressed or are very weakly expressed in U937 cells (44). In our study, we made use of this finding and employed the nonspecific FABP inhibitor BMS309403 to inhibit AEA uptake. We obtained a 10-fold lower IC_{50} value for AEA uptake inhibition in FABP-expressing cells (U937 macrophages) compared with the non-expressing cells (U937 cells). However, UCM707 and OMDM-2 inhibited AEA uptake in both cell types with the same potency, independent of FABP expression. This finding confirms the involvement of FABPs in the intracellular trafficking of AEA but also clearly refutes the hypothesis that these carrier proteins are the main target of EMT inhibitors. The inhibition of AEA uptake in FAAH-transfected HeLa cells shown by Kaczocha *et al.* (61) could be derived from a partial FAAH inhibition rather than the exclusive interaction with FABPs, due to the high EMT inhibitor concentrations applied. On the other hand, the loss of AEA uptake in FABP-deficient cells could be the consequence of the disruption of the AEA movement toward the ER, reflecting the participation of FABPs in AEA intracellular trafficking. Although FABPs have been proposed to possess promiscuous binding pockets for several endocannabinoid-like molecules, 2-AG binding has not been shown so far (61).

Another major concern about the specificity of the uptake inhibitors toward the EMT over other ECS targets, such as intracellular carriers and FAAH, is related to the kinetics of cellular AEA uptake. Some studies report that uptake inhibition occurs only at late time points (*i.e.* later than 90 s of incubation) (24, 25), whereas most of the measurements on cellular AEA uptake have been carried out after 4–10 min of incubation, thus raising the question of the role of downstream targets in the AEA uptake inhibition (12). In our hands, the inhibition of [^{3}H]AEA cellular uptake by UCM707 and OMDM-2 was identical from 30 s to 10 min, accounting for a very fast and constant transport process mediated by a cell membrane target rather than intracellular targets. Furthermore, the EMT inhibitor concentrations applied were significantly lower than the ones required for FAAH inhibition (Refs. 19 and 20 and this work) or AIBP binding (11, 61).

Evidence That AEA and 2-AG Share a Common Membrane Transport Mechanism—Our results clearly point out that the EMT is a membrane transporter for both AEA and 2-AG. However, intracellular carriers have so far only been identified for AEA (9–11), and unlike with AEA, relatively little is known about the trafficking of 2-AG across the cellular membrane (28). A few studies have reported 2-AG uptake via a protein-facilitated mechanism that is shared by AEA (29–32). 2-AG was shown to inhibit AEA uptake in C6 rat glioma cells with an IC_{50} value of 4.6 μM, whereas, in the same setting, AEA was not able to significantly modulate 2-AG uptake at 20-fold higher concentrations (31). Similarly, the competitive effect of 2-AG on cellular AEA uptake has been described with similar potency in RBL-2H3 rat basophilic leukemia cells (92) and Neuro-2a mouse neuroblastoma cells (65), as well as in granule and astrocytoma cells (33, 93). In addition, several papers (30–35, 39, 64) have reported 2-AG uptake to possess the typical characteristics of a carrier-mediated transport, such as time and temperature dependence, saturability, and sensitivity to the nonspecific AEA transport inhibitor AM404 in different cell lines. Despite these results, it is still debated whether the same putative transporter is responsible for both AEA and 2-AG uptake because only 2-AG was shown to inhibit AEA trafficking at physiological concentration ratios between the two endocannabinoids (31). To our knowledge, so far only two EMT inhibitors have been tested on 2-AG uptake, namely AM404 (30, 31, 35) and its 2-methylphenyl derivative, VDM11 (34). At 10 μM, both compounds inhibit cellular 2-AG uptake, but both compounds also target other proteins, such as the transient receptor potential vanilloid type 1 (TRPV1) (94), membrane channels (95–97), FLAT (11), FAPBs (61), FAAH (93), MAGL (98), and others (99). Other researchers did not report any interplay between cellular AEA and 2-AG uptake but suggested that the latter is mediated either via a passive diffusion process (29, 100) or by a specific transporter (different from AEA). All of the experiments carried out so far relied on the radiolabeled 2-AG, without quantifying the absolute amounts of the endocannabinoid intra- and extracellularly. Exact assay conditions (*i.e.* low endocannabinoid concentrations and short incubation times) and controls (unambiguous signal detection) seem mandatory to be able to measure endocannabinoid membrane transport. Here we clearly show a reciprocal competition between AEA and 2-AG membrane trafficking at physiological concentration ratios (2-AG up to 50 times higher than AEA and AEA up to 5 times higher than 2-AG (101)). In particular, 2-AG inhibited AEA uptake at a 10:1 concentration ratio, whereas AEA elicited the same effect at a 5:1 concentration ratio. Although the two endocannabinoids mutually inhibited their uptake at physiological concentration ratios, an estimated factor 2 of difference in favor of AEA was recognized, supporting a higher affinity of AEA toward the EMT. Furthermore, both UCM707 and OMDM-2 inhibited 2-AG uptake with IC_{50} values similar to AEA uptake inhibition. In agreement with the absence of [^{3}H]glycerol incorporation into PLs, the effect of JZL184 was a concentration-dependent increase of the intracellular 2-AG level. When UCM707 was combined with increasing concentrations of JZL184, the intracellular accumulation of 2-AG was inhibited, implying that less 2-AG can enter the cells. Unlike for AEA, both EMT inhibitors did not lead to an increase of the 2-AG extracellular level and to a reduction of the glycerol formation. This difference can be explained by the more complex degrading machinery involved in 2-AG breakdown, which involves at least three distinct enzymes located in the cell membrane. In addition to MAGL (81, 102), which is usually found associated with the inner cell membrane leaflet, two other hydrolyzes have been recently identified to hydrolyze 2-AG, ABHD-6 and -12. It is noteworthy that these enzymes are integral cell membrane proteins that have been suggested to share

the catalytic triad with MAGL (8). ABHD-6 has been proposed to face the catalytic site intracellularly and ABHD-12 extracellularly (58, 59). The physiological relevance of this redundancy of 2-AG breakdown is still being investigated, but it appears completely different from AEA, whose enzymatic inactivation is primarily mediated by the ER-located FAAH (3). Therefore, in our system, the extracellular accumulation of 2-AG is probably lowered by the hydrolytic activity of ABHDs, as suggested also by the higher levels of glycerol formation. Although these enzymes have so far been identified only in the brain and in neuronal cell lines, a recent study showed a high expression of both ABHDs in mouse macrophages (103). In agreement, we show that ABHD-6 and ABHD-12 transcripts are expressed in both U937 cells and U937 macrophages.

Toward a Common Membrane Transport Mechanism for Arachidonoyl Chain Harboring Endocannabinoids—We found that the *N*-acylethanolamines PEA, OEA, LEA, and SEA, which have been reported to be co-released with the endocannabinoid AEA upon cellular stimulation, did not influence the uptake of AEA and 2-AG. The cellular uptake of PEA and SEA has already been shown to be independent from cellular AEA uptake (65, 66). We show that the three additional arachidonoyl chain-containing endocannabinoids (eicosanoids), NADA, virodhamine, and noladin ether, compete with the uptake of AEA and 2-AG in U937 cells, independent of their ability to inhibit FAAH and MAGL. NADA has previously been shown to inhibit [^{14}C]AEA uptake in RBL-2H3 and C6 glioma cells with IC_{50} values of 21.5 and 17.5 μM, respectively (104) and to inhibit FAAH (IC_{50} values of 22.0 and 23.0 μM in N18TG2 cells and RBL-2H3 cells, respectively) (104) and MAGL (IC_{50} value of 0.78 μM in rat cerebellar homogenate) (98). Conversely, noladin ether was shown to inhibit [^{14}C]AEA and [^{3}H]2-AG uptake in C6 glioma cells with IC_{50} values of 15.6 and 22.7 μM, respectively (105) and to inhibit FAAH with an IC_{50} value of 3 μM in rat cerebellar homogenate without significantly inhibiting MAGL (IC_{50} 36 μM in rat cerebellar homogenate) (106). To date, little is known about virodhamine. In agreement with our finding, it has been found to inhibit [^{14}C]AEA uptake with a relatively high IC_{50} value (123 μM) in RBL-2H3 cells (107). It must be considered that different cells may express the putative EMT to different degrees, and depending on the amount of AEA added in each assay, also passive diffusion and FABPs could play a role. Our observation that arachidonoyl chain-containing endocannabinoids compete for the cellular uptake of [^{3}H]AEA and [^{3}H]2-AG but not other *N*-acylethanolamines suggests a common membrane transport mechanism for endocannabinoids, pinpointing the importance of the arachidonoyl moiety for competition. This is in agreement with a previous conclusion on the importance of the arachidonoyl moiety for AEA transport inhibitors (73, 108).

Evidence for the Involvement of the EMT in the Cellular Release of AEA and 2-AG—A pivotal characteristic for an energy-independent carrier-mediated transporter is the bidirectional shuttling of the substrate across the cell membrane, depending on the concentration gradient. Only very few papers have addressed this issue with AEA transport. Ligresti *et al.* (16) showed a reduction of AEA release upon thapsigargin stimulation in HEK293 cells and in dorsal root ganglion neurons when preincubated with 4 μM VDM11. In another experiment, Maccarrone *et al.* (37) reported a similar inhibition of release of preloaded [^{3}H]AEA from HUVEC cells when preincubated with 10 μM AM404. In the same article, the *trans*-effect of flux coupling has also been reported, measuring accumulation of [^{3}H]AEA added to HUVEC cells preloaded with 100 μM "cold" AEA (37). Similarly, a time- and temperature-dependent AEA efflux was shown in cerebellar granule cells preloaded with radiolabeled [^{3}H]AEA (38). In the same cells, Hillard and Jarrahian (39) demonstrated that the transcellular movement of AEA exhibits the *trans*-effect of flux coupling. Our results now demonstrate that all of the three inhibitors tested, UCM707, OMDM-2, and LY2183240, produced a concentration-dependent reduction of the endocannabinoid release coupled with an increase of the intracellular levels. We therefore not only confirmed the presence of a carrier-mediated bidirectional [^{3}H]AEA movement across the cell membrane but also show that structurally unrelated inhibitors of AEA cellular uptake partially block [^{3}H]AEA. The maximal inhibition of [^{3}H]AEA release was in the range of 20–40%, whereas its intracellular level increased by 50–80%. This difference could be explained by the presence of different intracellular storage compartments that remove [^{3}H]AEA from the cytosolic pool, which is released following an outward concentration gradient. To our knowledge, there is so far no literature addressing the mechanism involved in 2-AG release. Therefore, we have applied the same methodology to assess 2-AG cellular efflux in U937 cells, using a combination of inhibitors of 2-AG degradation (JZL184 for MAGL (109), WWL70 for ABHD-6 (110), and tetrahydrolipstatin for ABHD-12 (8)). Tetrahydrolipstatin also inhibits diacylglycerol lipase (the main enzyme involved in the 2-AG biosynthesis) with a higher potency than for ABHD-12 (111). Thus, at the concentration used in our assay, a potential *de novo* synthesis of 2-AG can be excluded. By using this method, we were able, for the first time, to show that the same small molecule inhibitors that lead to a reduction of AEA and 2-AG uptake are also able to inhibit the release of both endocannabinoids, resulting in a parallel increase of their intracellular levels. Because the mechanism of endocannabinoid release has not yet been elucidated, our consistent evidence for the bidirectionality of the putative EMT may provide the basis for future research. Our findings further suggest several intriguing physiological scenarios as it has more recently become evident that endocannabinoids have several intracellular targets, including nuclear PPARs, the membrane TRPV channels, and intracellular cannabinoid receptors (112, 113). Along this line, a recent study identified and characterized the presence of functional CB_1 receptors on the mitochondria (mtCB1) in mice hippocampal neurons (113). Furthermore, for 2-AG a novel positive allosteric $GABA_A$ receptor binding site at the inner leaflet of the cell membrane has been identified (114).

Altogether, our findings suggest that the putative EMT may be the only common target between AEA and 2-AG in the trafficking and metabolism pathways. While AEA binds to AIPBs and is shuttled to several intracellular sites, such as the inner cell membrane leaflet (TRPV1), nuclear membrane (PPARs), ER (FAAH-1), and adiposomes (FAAH-2), to date no intracellular carrier proteins have been shown to bind and/or shuttle

2-AG. Furthermore, AEA is primarily hydrolyzed by the ER-located FAAH, whereas 2-AG breakdown occurs at the cell membrane, where MAGL and the newly identified integral ABHD enzymes are located. Unlike FAAH or MAGL inhibitors, endocannabinoid membrane transport inhibitors could shift the endocannabinoid response toward either extracellular or intracellular targets, depending on the overall expression context. The latter possibility seems to be quite appealing in the light of the pleiotropic effects triggered by AEA through interaction with intracellular targets, such as inflammation modulation (PPARs) and nociception (TRPV1). In conclusion, our data provide new evidence in favor of a common cell membrane-associated mechanism for the cellular release and uptake of the major endocannabinoids in U937 cells. Specific inhibitors for this endocannabinoid cell membrane transport mechanism hold great potential as novel modulators of the ECS, which probably modulate endocannabinoid action differently from inhibitors of FAAH and MAGL.

Acknowledgments—We thank Bararba Adinolfi for assistance with the PCR analysis and Peter Bütikofer for assistance with the TLC analyses and for kindly providing PE, PS, PC, and ethanolamine.

REFERENCES

1. Di Marzo, V. (2008) Targeting the endocannabinoid system. To enhance or reduce? *Nat. Rev. Drug Discov.* **7,** 438–455
2. Battista, N., Di Tommaso, M., Bari, M., and Maccarrone, M. (2012) The endocannabinoid system. An overview. *Front. Behav. Neurosci.* **6,** 9
3. Cravatt, B. F., Giang, D. K., Mayfield, S. P., Boger, D. L., Lerner, R. A., and Gilula, N. B. (1996) Molecular characterization of an enzyme that degrades neuromodulatory fatty acid amides. *Nature* **384,** 83–87
4. Dinh, T. P., Carpenter, D., Leslie, F. M., Freund, T. F., Katona, I., Sensi, S. L., Kathuria, S., and Piomelli, D. (2002) Brain monoglyceride lipase participating in endocannabinoid inactivation. *Proc. Natl. Acad. Sci. U.S.A.* **99,** 10819–10824
5. Ueda, N., Yamanaka, K., and Yamamoto, S. (2001) Purification and characterization of an acid amidase selective for *N*-palmitoylethanolamine, a putative endogenous anti-inflammatory substance. *J. Biol. Chem.* **276,** 35552–35557
6. Ueda, N., Yamanaka, K., Terasawa, Y., and Yamamoto, S. (1999) An acid amidase hydrolyzing anandamide as an endogenous ligand for cannabinoid receptors. *FEBS Lett.* **454,** 267–270
7. Wei, B. Q., Mikkelsen, T. S., McKinney, M. K., Lander, E. S., and Cravatt, B. F. (2006) A second fatty acid amide hydrolase with variable distribution among placental mammals. *J. Biol. Chem.* **281,** 36569–36578
8. Blankman, J. L., Simon, G. M., and Cravatt, B. F. (2007) A comprehensive profile of brain enzymes that hydrolyze the endocannabinoid 2-arachidonoylglycerol. *Chem. Biol.* **14,** 1347–1356
9. Kaczocha, M., Glaser, S. T., and Deutsch, D. G. (2009) Identification of intracellular carriers for the endocannabinoid anandamide. *Proc. Natl. Acad. Sci. U.S.A.* **106,** 6375–6380
10. Oddi, S., Fezza, F., Pasquariello, N., D'Agostino, A., Catanzaro, G., De Simone, C., Rapino, C., Finazzi-Agrò, A., and Maccarrone, M. (2009) Molecular identification of albumin and Hsp70 as cytosolic anandamide-binding proteins. *Chem. Biol.* **16,** 624–632
11. Fu, J., Bottegoni, G., Sasso, O., Bertorelli, R., Rocchia, W., Masetti, M., Guijarro, A., Lodola, A., Armirotti, A., Garau, G., Bandiera, T., Reggiani, A., Mor, M., Cavalli, A., and Piomelli, D. (2012) A catalytically silent FAAH-1 variant drives anandamide transport in neurons. *Nat. Neurosci.* **15,** 64–69
12. Fowler, C. J. (2012) Anandamide uptake explained? *Trends Pharmacol. Sci.* **33,** 181–185
13. Felder, C. C., Dickason-Chesterfield, A. K., and Moore, S. A. (2006) Cannabinoid biology. The search for new therapeutic targets. *Mol. Interv.* **6,** 149–161
14. Moore, S. A., Nomikos, G. G., Dickason-Chesterfield, A. K., Schober, D. A., Schaus, J. M., Ying, B. P., Xu, Y. C., Phebus, L., Simmons, R. M., Li, D., Iyengar, S., and Felder, C. C. (2005) Identification of a high affinity binding site involved in the transport of endocannabinoids. *Proc. Natl. Acad. Sci. U.S.A.* **102,** 17852–17857
15. Ligresti, A., De Petrocellis, L., Hernán Pérez de la Ossa, D., Aberturas, R., Cristino, L., Moriello, A. S., Finizio, A., Gil, M. E., Torres, A. I., Molpeceres, J., and Di Marzo, V. (2010) Exploiting nanotechnologies and TRPV1 channels to investigate the putative anandamide membrane transporter. *PloS One* **5,** e10239
16. Ligresti, A., Morera, E., Van Der Stelt, M., Monory, K., Lutz, B., Ortar, G., and Di Marzo, V. (2004) Further evidence for the existence of a specific process for the membrane transport of anandamide. *Biochem. J.* **380,** 265–272
17. Di Marzo, V., Fontana, A., Cadas, H., Schinelli, S., Cimino, G., Schwartz, J. C., and Piomelli, D. (1994) Formation and inactivation of endogenous cannabinoid anandamide in central neurons. *Nature* **372,** 686–691
18. Deutsch, D. G., Glaser, S. T., Howell, J. M., Kunz, J. S., Puffenbarger, R. A., Hillard, C. J., and Abumrad, N. (2001) The cellular uptake of anandamide is coupled to its breakdown by fatty acid amide hydrolase. *J. Biol. Chem.* **276,** 6967–6973
19. Ortar, G., Ligresti, A., De Petrocellis, L., Morera, E., and Di Marzo, V. (2003) Novel selective and metabolically stable inhibitors of anandamide cellular uptake. *Biochem. Pharmacol.* **65,** 1473–1481
20. López-Rodríguez, M. L., Viso, A., Ortega-Gutiérrez, S., Fowler, C. J., Tiger, G., de Lago, E., Fernández-Ruiz, J., and Ramos, J. A. (2003) Design, synthesis, and biological evaluation of new endocannabinoid transporter inhibitors. *Eur. J. Med. Chem.* **38,** 403–412
21. De Petrocellis, L., Bisogno, T., Davis, J. B., Pertwee, R. G., and Di Marzo, V. (2000) Overlap between the ligand recognition properties of the anandamide transporter and the VR1 vanilloid receptor. Inhibitors of anandamide uptake with negligible capsaicin-like activity. *FEBS Lett.* **483,** 52–56
22. Day, T. A., Rakhshan, F., Deutsch, D. G., and Barker, E. L. (2001) Role of fatty acid amide hydrolase in the transport of the endogenous cannabinoid anandamide. *Mol. Pharmacol.* **59,** 1369–1375
23. Fasia, L., Karava, V., and Siafaka-Kapadai, A. (2003) Uptake and metabolism of [^{3}H]anandamide by rabbit platelets. Lack of transporter? *Eur. J. Biochem.* **270,** 3498–3506
24. Glaser, S. T., Abumrad, N. A., Fatade, F., Kaczocha, M., Studholme, K. M., and Deutsch, D. G. (2003) Evidence against the presence of an anandamide transporter. *Proc. Natl. Acad. Sci. U.S.A.* **100,** 4269–4274
25. Kaczocha, M., Hermann, A., Glaser, S. T., Bojesen, I. N., and Deutsch, D. G. (2006) Anandamide uptake is consistent with rate-limited diffusion and is regulated by the degree of its hydrolysis by fatty acid amide hydrolase. *J. Biol. Chem.* **281,** 9066–9075
26. McFarland, M. J., Bardell, T. K., Yates, M. L., Placzek, E. A., and Barker, E. L. (2008) RNA interference-mediated knockdown of dynamin 2 reduces endocannabinoid uptake into neuronal dCAD cells. *Mol. Pharmacol.* **74,** 101–108
27. McFarland, M. J., Porter, A. C., Rakhshan, F. R., Rawat, D. S., Gibbs, R. A., and Barker, E. L. (2004) A role for caveolae/lipid rafts in the uptake and recycling of the endogenous cannabinoid anandamide. *J. Biol. Chem.* **279,** 41991–41997
28. Fowler, C. J., and Ghafouri, N. (2008) Does the hydrolysis of 2-arachidonoylglycerol regulate its cellular uptake? *Pharmacol. Res.* **58,** 72–76
29. Hermann, A., Kaczocha, M., and Deutsch, D. G. (2006) 2-Arachidonoylglycerol (2-AG) membrane transport. History and outlook. *AAPS J.* **8,** E409–E412
30. Beltramo, M., and Piomelli, D. (2000) Carrier-mediated transport and enzymatic hydrolysis of the endogenous cannabinoid 2-arachidonylglycerol. *Neuroreport* **11,** 1231–1235
31. Bisogno, T., MacCarrone, M., De Petrocellis, L., Jarrahian, A., Finazzi-Agrò, A., Hillard, C., and Di Marzo, V. (2001) The uptake by cells of 2-arachidonoylglycerol, an endogenous agonist of cannabinoid receptors. *Eur. J. Biochem.* **268,** 1982–1989

32. Hillard, C. J., and Jarrahian, A. (2003) Cellular accumulation of anandamide. Consensus and controversy. *Br. J. Pharmacol.* **140,** 802–808
33. Piomelli, D., Beltramo, M., Glasnapp, S., Lin, S. Y., Goutopoulos, A., Xie, X. Q., and Makriyannis, A. (1999) Structural determinants for recognition and translocation by the anandamide transporter. *Proc. Natl. Acad. Sci. U.S.A.* **96,** 5802–5807
34. Bari, M., Spagnuolo, P., Fezza, F., Oddi, S., Pasquariello, N., Finazzi-Agrò, A., and Maccarrone, M. (2006) Effect of lipid rafts on Cb2 receptor signaling and 2-arachidonoyl-glycerol metabolism in human immune cells. *J. Immunol.* **177,** 4971–4980
35. Hájos, N., Kathuria, S., Dinh, T., Piomelli, D., and Freund, T. F. (2004) Endocannabinoid transport tightly controls 2-arachidonoyl glycerol actions in the hippocampus. Effects of low temperature and the transport inhibitor AM404. *Eur. J. Neurosci.* **19,** 2991–2996
36. Di Marzo, V., De Petrocellis, L., and Bisogno, T. (2005) The biosynthesis, fate, and pharmacological properties of endocannabinoids. *Handb. Exp. Pharmacol.* **1,** 147–185
37. Maccarrone, M., Bari, M., Battista, N., and Finazzi-Agrò, A. (2002) Estrogen stimulates arachidonoylethanolamide release from human endothelial cells and platelet activation. *Blood* **100,** 4040–4048
38. Hillard, C. J., Edgemond, W. S., Jarrahian, A., and Campbell, W. B. (1997) Accumulation of *N*-arachidonoylethanolamine (anandamide) into cerebellar granule cells occurs via facilitated diffusion. *J. Neurochem.* **69,** 631–638
39. Hillard, C. J., and Jarrahian, A. (2000) The movement of *N*-arachidonoylethanolamine (anandamide) across cellular membranes. *Chem. Phys. Lipids* **108,** 123–134
40. Oddi, S., Fezza, F., Catanzaro, G., De Simone, C., Pucci, M., Piomelli, D., Finazzi-Agrò, A., and Maccarrone, M. (2010) Pitfalls and solutions in assaying anandamide transport in cells. *J. Lipid Res.* **51,** 2435–2444
41. Fowler, C. J., Tiger, G., Ligresti, A., López-Rodríguez, M. L., and Di Marzo, V. (2004) Selective inhibition of anandamide cellular uptake versus enzymatic hydrolysis. A difficult issue to handle. *Eur. J. Pharmacol.* **492,** 1–11
42. Izeboud, C. A., Vermeulen, R. M., Zwart, A., Voss, H. P., van Miert, A. S., and Witkamp, R. F. (2000) Stereoselectivity at the beta2-adrenoceptor on macrophages is a major determinant of the anti-inflammatory effects of beta2-agonists. *Naunyn Schmiedebergs Arch. Pharmacol.* **362,** 184–189
43. Nievergelt, A., Marazzi, J., Schoop, R., Altmann, K. H., and Gertsch, J. (2011) Ginger phenylpropanoids inhibit IL-1β and prostanoid secretion and disrupt arachidonate-phospholipid remodeling by targeting phospholipases A2. *J. Immunol.* **187,** 4140–4150
44. Verhoeckx, K. C., Bijlsma, S., de Groene, E. M., Witkamp, R. F., van der Greef, J., and Rodenburg, R. J. (2004) A combination of proteomics, principal component analysis and transcriptomics is a powerful tool for the identification of biomarkers for macrophage maturation in the U937 cell line. *Proteomics* **4,** 1014–1028
45. Pöch, G., and Holzmann, S. (1980) Quantitative estimation of overadditive and underadditive drug effects by means of theoretical, additive dose-response curves. *J. Pharmacol. Methods* **4,** 179–188
46. Pöch, G., Dittrich, P., and Holzmann, S. (1990a) Evaluation of combined effects in dose-response studies by statistical comparison with additive and independent interactions. *J. Pharmacol. Methods* **24,** 311–325
47. Pöch, G., Dittrich, P., Reiffenstein, R. J., Lenk, W., and Schuster, A. (1990) Evaluation of experimental combined toxicity by use of dose-frequency curves. Comparison with theoretical additivity as well as independence. *Can. J. Physiol. Pharmacol.* **68,** 1338–1345
48. Pöch, G., Reiffenstein, R. J., and Baer, H. P. (1995) Quantitative estimation of potentiation and antagonism by dose ratios corrected for slopes of dose-response curves deviating from one. *J. Pharmacol. Toxicol. Methods* **33,** 197–204
49. Chicca, A., Raduner, S., Pellati, F., Strompen, T., Altmann, K. H., Schoop, R., and Gertsch, J. (2009) Synergistic immunomopharmacological effects of *N*-alkylamides in *Echinacea purpurea* herbal extracts. *Int. Immunopharmacol.* **9,** 850–858
50. Marazzi, J., Kleyer, J., Paredes, J. M., and Gertsch, J. (2011) Endocannabinoid content in fetal bovine sera. Unexpected effects on mononuclear cells and osteoclastogenesis. *J. Immunol. Methods* **373,** 219–228
51. Folch, J., Lees, M., and Sloane Stanley, G. H. (1957) A simple method for the isolation and purification of total lipides from animal tissues. *J. Biol. Chem.* **226,** 497–509
52. Obata, T., Sakurai, Y., Kase, Y., Tanifuji, Y., and Horiguchi, T. (2003) Simultaneous determination of endocannabinoids (arachidonylethanolamide and 2-arachidonylglycerol) and isoprostane (8-epiprostaglandin F2α) by gas chromatography-mass spectrometry-selected ion monitoring for medical samples. *J. Chromatogr. B Analyt. Technol. Biomed. Life Sci.* **792,** 131–140
53. Schmid, P. C., Schwartz, K. D., Smith, C. N., Krebsbach, R. J., Berdyshev, E. V., and Schmid, H. H. (2000) A sensitive endocannabinoid assay. The simultaneous analysis of *N*-acylethanolamines and 2-monoacylglycerols. *Chem. Phys. Lipids.* **104,** 185–191
54. Fogli, S., Nieri, P., Chicca, A., Adinolfi, B., Mariotti, V., Iacopetti, P., Breschi, M. C., and Pellegrini, S. (2006) Cannabinoid derivatives induce cell death in pancreatic MIA PaCa-2 cells via a receptor-independent mechanism. *FEBS Lett.* **580,** 1733–1739
55. Maccarrone, M., van der Stelt, M., Rossi, A., Veldink, G. A., Vliegenthart, J. F., and Finazzi-Agrò, A. F. (1998) Anandamide hydrolysis by human cells in culture and brain. *J. Biol. Chem.* **273,** 32332–32339
56. Kathuria, S., Gaetani, S., Fegley, D., Valiño, F., Duranti, A., Tontini, A., Mor, M., Tarzia, G., La Rana, G., Calignano, A., Giustino, A., Tattoli, M., Palmery, M., Cuomo, V., and Piomelli, D. (2003) Modulation of anxiety through blockade of anandamide hydrolysis. *Nat. Med.* **9,** 76–81
57. Deutsch, D. G., and Chin, S. A. (1993) Enzymatic synthesis and degradation of anandamide, a cannabinoid receptor agonist. *Biochem. Pharmacol.* **46,** 791–796
58. Ahn, K., McKinney, M. K., and Cravatt, B. F. (2008) Enzymatic pathways that regulate endocannabinoid signaling in the nervous system. *Chem. Rev.* **108,** 1687–1707
59. Savinainen, J. R., Saario, S. M., and Laitinen, J. T. (2012) The serine hydrolases MAGL, ABHD6, and ABHD12 as guardians of 2-arachidonoylglycerol signalling through cannabinoid receptors. *Acta Physiol.* **204,** 267–276
60. Maccarrone, M., Dainese, E., and Oddi, S. (2010) Intracellular trafficking of anandamide. New concepts for signaling. *Trends Biochem. Sci.* **35,** 601–608
61. Kaczocha, M., Vivieca, S., Sun, J., Glaser, S. T., and Deutsch, D. G. (2012) Fatty acid-binding proteins transport *N*-acylethanolamines to nuclear receptors and are targets of endocannabinoid transport inhibitors. *J. Biol. Chem.* **287,** 3415–3424
62. Sulsky, R., Magnin, D. R., Huang, Y., Simpkins, L., Taunk, P., Patel, M., Zhu, Y., Stouch, T. R., Bassolino-Klimas, D., Parker, R., Harrity, T., Stoffel, R., Taylor, D. S., Lavoie, T. B., Kish, K., Jacobson, B. L., Sheriff, S., Adam, L. P., Ewing, W. R., and Robl, J. A. (2007) Potent and selective biphenyl azole inhibitors of adipocyte fatty acid-binding protein (aFABP). *Bioorg. Med. Chem. Lett.* **17,** 3511–3515
63. McFarland, M. J., and Barker, E. L. (2004) Anandamide transport. *Pharmacol. Ther.* **104,** 117–135
64. Di Marzo, V., Bisogno, T., De Petrocellis, L., Melck, D., Orlando, P., Wagner, J. A., and Kunos, G. (1999) Biosynthesis and inactivation of the endocannabinoid 2-arachidonoylglycerol in circulating and tumoral macrophages. *Eur. J. Biochem.* **264,** 258–267
65. Jacobsson, S. O., and Fowler, C. J. (2001) Characterization of palmitoylethanolamide transport in mouse Neuro-2a neuroblastoma and rat RBL-2H3 basophilic leukaemia cells. Comparison with anandamide. *Br. J. Pharmacol.* **132,** 1743–1754
66. Maccarrone, M., Pauselli, R., Di Rienzo, M., and Finazzi-Agrò, A. (2002) Binding, degradation, and apoptotic activity of stearoylethanolamide in rat C6 glioma cells. *Biochem. J.* **366,** 137–144
67. La Rana, G., Russo, R., Campolongo, P., Bortolato, M., Mangieri, R. A., Cuomo, V., Iacono, A., Raso, G. M., Meli, R., Piomelli, D., and Calignano, A. (2006) Modulation of neuropathic and inflammatory pain by the endocannabinoid transport inhibitor AM404. *J. Pharmacol. Exp. Ther.* **317,** 1365–1371
68. Maione, S., Morera, E., Marabese, I., Ligresti, A., Luongo, L., Ortar, G., and Di Marzo, V. (2008) Antinociceptive effects of tetrazole inhibitors of endocannabinoid inactivation. Cannabinoid and non-cannabinoid re-

ceptor-mediated mechanisms. *Br. J. Pharmacol.* **155,** 775–782
69. La Rana, G., Russo, R., D'Agostino, G., Sasso, O., Raso, G. M., Iacono, A., Meli, R., Piomelli, D., and Calignano, A. (2008) AM404, an anandamide transport inhibitor, reduces plasma extravasation in a model of neuropathic pain in rat. Role for cannabinoid receptors. *Neuropharmacology* **54,** 521–529
70. Costa, B., Siniscalco, D., Trovato, A. E., Comelli, F., Sotgiu, M. L., Colleoni, M., Maione, S., Rossi, F., and Giagnoni, G. (2006) AM404, an inhibitor of anandamide uptake, prevents pain behavior and modulates cytokine and apoptotic pathways in a rat model of neuropathic pain. *Br. J. Pharmacol.* **148,** 1022–1032
71. Yates, M. L., and Barker, E. L. (2009) Inactivation and biotransformation of the endogenous cannabinoids anandamide and 2-arachidonoylglycerol. *Mol. Pharmacol.* **76,** 11–17
72. Bisogno, T., Ligresti, A., and Di Marzo, V. (2005) The endocannabinoid signaling system. Biochemical aspects. *Pharmacol. Biochem. Behav.* **81,** 224–238
73. Oddi, S., Fezza, F., Pasquariello, N., De Simone, C., Rapino, C., Dainese, E., Finazzi-Agrò, A., and Maccarrone, M. (2008) Evidence for the intracellular accumulation of anandamide in adiposomes. *Cell Mol. Life Sci.* **65,** 840–850
74. Hamtiaux, L., Hansoulle, L., Dauguet, N., Muccioli, G. G., Gallez, B., and Lambert, D. M. (2011) Increasing antiproliferative properties of endocannabinoids in N1E-115 neuroblastoma cells through inhibition of their metabolism. *PloS One* **6,** e26823
75. Piomelli, D., Tarzia, G., Duranti, A., Tontini, A., Mor, M., Compton, T. R., Dasse, O., Monaghan, E. P., Parrott, J. A., and Putman, D. (2006) Pharmacological profile of the selective FAAH inhibitor KDS-4103 (URB597). *CNS Drug Rev.* **12,** 21–38
76. Thors, L., Eriksson, J., and Fowler, C. J. (2007) Inhibition of the cellular uptake of anandamide by genistein and its analogue daidzein in cells with different levels of fatty acid amide hydrolase-driven uptake. *Br. J. Pharmacol.* **152,** 744–750
77. Blom, T., Somerharju, P., and Ikonen, E. (2011) Synthesis and biosynthetic trafficking of membrane lipids. *Cold Spring Harb. Perspect. Biol.* **3,** a004713
78. Vance, J. E. (2008) Phosphatidylserine and phosphatidylethanolamine in mammalian cells. Two metabolically related aminophospholipids. *J. Lipid Res.* **49,** 1377–1387
79. Gallego-Ortega, D., Ramirez de Molina, A., Ramos, M. A., Valdes-Mora, F., Barderas, M. G., Sarmentero-Estrada, J., and Lacal, J. C. (2009) Differential role of human choline kinase α and β enzymes in lipid metabolism. Implications in cancer onset and treatment. *PloS One* **4,** e7819
80. Chu, A. J., Nguyen, C. T., and Moore, J. (1993) Differential effects of unsaturated fatty acids on phospholipid synthesis in human leukemia monocytic U937 cells. *Cell Biochem. Funct.* **11,** 201–209
81. Labar, G., Bauvois, C., Borel, F., Ferrer, J. L., Wouters, J., and Lambert, D. M. (2010) Crystal structure of the human monoacylglycerol lipase, a key actor in endocannabinoid signaling. *Chembiochem* **11,** 218–227
82. Rojek, A., Praetorius, J., Frøkiaer, J., Nielsen, S., and Fenton, R. A. (2008) A current view of the mammalian aquaglyceroporins. *Annu. Rev. Physiol.* **70,** 301–327
83. Liu, Y., Song, L., Wang, Y., Rojek, A., Nielsen, S., Agre, P., and Carbrey, J. M. (2009) Osteoclast differentiation and function in aquaglyceroporin AQP9-null mice. *Biol. Cell* **101,** 133–140
84. Zhu, N., Feng, X., He, C., Gao, H., Yang, L., Ma, Q., Guo, L., Qiao, Y., Yang, H., and Ma, T. (2011) Defective macrophage function in aquaporin-3 deficiency. *FASEB J.* **25,** 4233–4239
85. Centonze, D., Battista, N., Rossi, S., Mercuri, N. B., Finazzi-Agrò, A., Bernardi, G., Calabresi, P., and Maccarrone, M. (2004) A critical interaction between dopamine D2 receptors and endocannabinoids mediates the effects of cocaine on striatal GABAergic transmission. *Neuropsychopharmacology* **29,** 1488–1497
86. Maccarrone, M., Bari, M., Lorenzon, T., Bisogno, T., Di Marzo, V., and Finazzi-Agrò, A. (2000) Anandamide uptake by human endothelial cells and its regulation by nitric oxide. *J. Biol. Chem.* **275,** 13484–13492
87. Ortega-Gutiérrez, S., Hawkins, E. G., Viso, A., López-Rodríguez, M. L., and Cravatt, B. F. (2004) Comparison of anandamide transport in FAAH wild-type and knockout neurons. Evidence for contributions by both FAAH and the CB1 receptor to anandamide uptake. *Biochemistry* **43,** 8184–8190
88. Verhoeckx, K. C., Korthout, H. A., van Meeteren-Kreikamp, A. P., Ehlert, K. A., Wang, M., van der Greef, J., Rodenburg, R. J., and Witkamp, R. F. (2006) Unheated *Cannabis sativa* extracts and its major compound THC-acid have potential immunomodulating properties not mediated by CB1 and CB2 receptor coupled pathways. *Int. Immunopharmacol.* **6,** 656–665
89. Bouaboula, M., Rinaldi, M., Carayon, P., Carillon, C., Delpech, B., Shire, D., Le Fur, G., and Casellas, P. (1993) Cannabinoid-receptor expression in human leukocytes. *Eur. J. Biochem.* **214,** 173–180
90. De Petrocellis, L., Davis, J. B., and Di Marzo, V. (2001) Palmitoylethanolamide enhances anandamide stimulation of human vanilloid VR1 receptors. *FEBS Lett.* **506,** 253–256
91. De Petrocellis, L., Bisogno, T., Maccarrone, M., Davis, J. B., Finazzi-Agro, A., and Di Marzo, V. (2001) The activity of anandamide at vanilloid VR1 receptors requires facilitated transport across the cell membrane and is limited by intracellular metabolism. *J. Biol. Chem.* **276,** 12856–12863
92. Rakhshan, F., Day, T. A., Blakely, R. D., and Barker, E. L. (2000) Carrier-mediated uptake of the endogenous cannabinoid anandamide in RBL-2H3 cells. *J. Pharmacol. Exp. Ther.* **292,** 960–967
93. Jarrahian, A., Manna, S., Edgemond, W. S., Campbell, W. B., and Hillard, C. J. (2000) Structure-activity relationships among *N*-arachidonylethanolamine (Anandamide) headgroup analogues for the anandamide transporter. *J. Neurochem.* **74,** 2597–2606
94. Zygmunt, P. M., Chuang, H., Movahed, P., Julius, D., and Högestätt, E. D. (2000) The anandamide transport inhibitor AM404 activates vanilloid receptors. *Eur. J. Pharmacol.* **396,** 39–42
95. Nicholson, R. A., Liao, C., Zheng, J., David, L. S., Coyne, L., Errington, A. C., Singh, G., and Lees, G. (2003) Sodium channel inhibition by anandamide and synthetic cannabimimetics in brain. *Brain Res.* **978,** 194–204
96. Kelley, B. G., and Thayer, S. A. (2004) Anandamide transport inhibitor AM404 and structurally related compounds inhibit synaptic transmission between rat hippocampal neurons in culture independent of cannabinoid CB1 receptors. *Eur. J. Pharmacol.* **496,** 33–39
97. Alptekin, A., Galadari, S., Shuba, Y., Petroianu, G., and Oz, M. (2010) The effects of anandamide transport inhibitor AM404 on voltage-dependent calcium channels. *Eur. J. Pharmacol.* **634,** 10–15
98. Björklund, E., Norén, E., Nilsson, J., and Fowler, C. J. (2010) Inhibition of monoacylglycerol lipase by troglitazone, *N*-arachidonoyl dopamine and the irreversible inhibitor JZL184. Comparison of two different assays. *Br. J. Pharmacol.* **161,** 1512–1526
99. Trezza, V., and Vanderschuren, L. J. (2009) Divergent effects of anandamide transporter inhibitors with different target selectivity on social play behavior in adolescent rats. *J. Pharmacol. Exp. Ther.* **328,** 343–350
100. Di Marzo, V., Bisogno, T., Sugiura, T., Melck, D., and De Petrocellis, L. (1998) The novel endogenous cannabinoid 2-arachidonoylglycerol is inactivated by neuronal- and basophil-like cells. Connections with anandamide. *Biochem. J.* **331,** 15–19
101. Zoerner, A. A., Gutzki, F. M., Batkai, S., May, M., Rakers, C., Engeli, S., Jordan, J., and Tsikas, D. (2011) Quantification of endocannabinoids in biological systems by chromatography and mass spectrometry. A comprehensive review from an analytical and biological perspective. *Biochim. Biophys. Acta* **1811,** 706–723
102. Bertrand, T., Augé, F., Houtmann, J., Rak, A., Vallée, F., Mikol, V., Berne, P. F., Michot, N., Cheuret, D., Hoornaert, C., and Mathieu, M. (2010) Structural basis for human monoglyceride lipase inhibition. *J. Mol. Biol.* **396,** 663–673
103. Fiskerstrand, T., H'mida-Ben Brahim, D., Johansson, S., M'zahem, A., Haukanes, B. I., Drouot, N., Zimmermann, J., Cole, A. J., Vedeler, C., Bredrup, C., Assoum, M., Tazir, M., Klockgether, T., Hamri, A., Steen, V. M., Boman, H., Bindoff, L. A., Koenig, M., and Knappskog, P. M. (2010) Mutations in ABHD12 cause the neurodegenerative disease PHARC. An inborn error of endocannabinoid metabolism. *Am. J. Hum. Genet.* **87,** 410–417
104. Bisogno, T., Melck, D., Bobrov MYu, Gretskaya, N. M., Bezuglov, V. V.,

De Petrocellis, L., and Di Marzo, V. (2000) *N*-Acyl-dopamines. Novel synthetic CB_1 cannabinoid-receptor ligands and inhibitors of anandamide inactivation with cannabimimetic activity *in vitro* and *in vivo*. *Biochem. J.* **351,** 817–824

105. Fezza, F., Bisogno, T., Minassi, A., Appendino, G., Mechoulam, R., Di Marzo, V. (2002) Noladin ether, a putative novel endocannabinoid. Inactivation mechanisms and a sensitive method for its quantification in rat tissues. *FEBS Lett.* **513,** 294–298
106. Ghafouri, N., Tiger, G., Razdan, R. K., Mahadevan, A., Pertwee, R. G., Martin, B. R., and Fowler, C. J. (2004) Inhibition of monoacylglycerol lipase and fatty acid amide hydrolase by analogues of 2-arachidonoylglycerol. *Br. J. Pharmacol.* **143,** 774–784
107. Porter, A. C., Sauer, J. M., Knierman, M. D., Becker, G. W., Berna, M. J., Bao, J., Nomikos, G. G., Carter, P., Bymaster, F. P., Leese, A. B., and Felder, C. C. (2002) Characterization of a novel endocannabinoid, virodhamine, with antagonist activity at the CB1 receptor. *J. Pharmacol. Exp. Ther.* **301,** 1020–1024
108. Muthian, S., Nithipatikom, K., Campbell, W. B., and Hillard, C. J. (2000) Synthesis and characterization of a fluorescent substrate for the *N*-arachidonoylethanolamine (anandamide) transmembrane carrier. *J. Pharmacol. Exp. Ther.* **293,** 289–295
109. Long, J. Z., Li, W., Booker, L., Burston, J. J., Kinsey, S. G., Schlosburg, J. E., Pavón, F. J., Serrano, A. M., Selley, D. E., Parsons, L. H., Lichtman, A. H., and Cravatt, B. F. (2009) Selective blockade of 2-arachidonoylglycerol hydrolysis produces cannabinoid behavioral effects. *Nat. Chem. Biol.* **5,** 37–44
110. Marrs, W. R., Blankman, J. L., Horne, E. A., Thomazeau, A., Lin, Y. H., Coy, J., Bodor, A. L., Muccioli, G. G., Hu, S. S., Woodruff, G., Fung, S., Lafourcade, M., Alexander, J. P., Long, J. Z., Li, W., Xu, C., Möller, T., Mackie, K., Manzoni, O. J., Cravatt, B. F., and Stella, N. (2010) The serine hydrolase ABHD6 controls the accumulation and efficacy of 2-AG at cannabinoid receptors. *Nat. Neurosci.* **13,** 951–957
111. Sarnataro, D., Grimaldi, C., Pisanti, S., Gazzerro, P., Laezza, C., Zurzolo, C., and Bifulco, M. (2005) Plasma membrane and lysosomal localization of CB1 cannabinoid receptor are dependent on lipid rafts and regulated by anandamide in human breast cancer cells. *FEBS Lett.* **579,** 6343–6349
112. Brailoiu, G. C., Oprea, T. I., Zhao, P., Abood, M. E., and Brailoiu, E. (2011) Intracellular cannabinoid type 1 (CB1) receptors are activated by anandamide. *J. Biol. Chem.* **286,** 29166–29174
113. Bénard, G., Massa, F., Puente, N., Lourenço, J., Bellocchio, L., Soria-Gómez, E., Matias, I., Delamarre, A., Metna-Laurent, M., Cannich, A., Hebert-Chatelain, E., Mulle, C., Ortega-Gutiérrez, S., Martín-Fontecha, M., Klugmann, M., Guggenhuber, S., Lutz, B., Gertsch, J., Chaouloff, F., López-Rodríguez, M. L., Grandes, P., Rossignol, R., and Marsicano, G. (2012) Mitochondrial CB_1 receptors regulate neuronal energy metabolism. *Nat. Neurosci.* **15,** 558–564
114. Sigel, E., Baur, R., Rácz, I., Marazzi, J., Smart, T. G., Zimmer, A., and Gertsch, J. (2011) The major central endocannabinoid directly acts at $GABA_A$ receptors. *Proc. Natl. Acad. Sci. U.S.A.* **108,** 18150–18155